JOURNAL OF ENZYME INHIBITION AND MEDICINAL CHEMISTRY
2021, VOL. 36, NO. 1, 1093–1114
https://doi.org/10.1080/14756366.2021.1915303

Taylor & Francis
Taylor & Francis Group

RESEARCH PAPER

OPEN ACCESS Check for updates

Discovery of new VEGFR-2 inhibitors based on bis([1, 2, 4]triazolo)[4,3-*a*:3′,4′-*c*] quinoxaline derivatives as anticancer agents and apoptosis inducers

Nawaf A. Alsaif[a], Mohammed S. Taghour[b], Mohammed M. Alanazi[a], Ahmad J. Obaidullah[a], Abdulrahman A. Al-Mehizia[a], Manal M. Alanazi[a], Saleh Aldawas[a], Alaa Elwan[b] and Hazem Elkady[b]

[a]Department of Pharmaceutical Chemistry, College of Pharmacy, King Saud University, Riyadh, Saudi Arabia; [b]Pharmaceutical Medicinal Chemistry & Drug Design Department, Faculty of Pharmacy (Boys), Al-Azhar University, Cairo, Egypt

ABSTRACT

Herein, a new wave of bis([1, 2, 4]triazolo)[4,3-*a*:3′,4′-*c*]quinoxaline derivatives have been successfully designed and synthesised. The synthesised derivatives were biologically investigated for their cytotoxic activities against HepG2 and MCF-7. Also, the tested compounds were further examined *in vitro* for their VEGFR-2 inhibitory activity. The most promising derivative **23j** was further investigated for its apoptotic behaviour in HepG2 cell lines using flow cytometric and western-plot analyses. Additional *in-silico* studies were performed to predict how the synthesised compounds can bind to VEGFR-2 and to determine the drug-likeness profiling of these derivatives. The results revealed that compounds **23a**, **23i**, **23j**, **23l**, and **23n** displayed the highest antiproliferative activities against the two cell lines with IC_{50} values ranging from 6.4 to 19.4 μM. Furthermore, compounds **23a**, **23d**, **23h**, **23i**, **23j**, **23l**, **23 m**, and **23n** showed the highest VEGFR-2 inhibitory activities with IC_{50} values ranging from 3.7 to 11.8 nM, comparing to sorafenib (IC_{50} = 3.12 nM). Moreover, compound **23j** arrested the HepG2 cell growth at the G2/M phase and induced apoptosis by 40.12% compared to the control cells (7.07%). As well, such compound showed a significant increase in the level of caspase-3 (1.36-fold), caspase-9 (2.80-fold), and BAX (1.65-fold), and exhibited a significant decrease in Bcl-2 level (2.63-fold).

ARTICLE HISTORY
Received 3 March 2021
Revised 24 March 2021
Accepted 6 April 2021

KEYWORDS
Anticancer; apoptosis; bis([1,2,4]triazolo)[4,3-*a*:3′,4′-*c*]quinoxaline; molecular docking; VEGFR-2

1. Introduction

Cancer is a rebound system represented by unrestricted cell growth[1]. Cancer originates in the humanoid body from the buildup of genetic and epigenetic variations in the normal cells[2]. In spite of the huge efforts directed towards cancer treatment and prevention, cancer remains one of the foremost public health problems all over the world[3]. Consequently; increasing interest in the current medicinal chemistry has been dedicated to the design and synthesis of more effective anticancer agents with low side effects[4].

Angiogenesis is a multi-stage process to produce new vessels from quiescent pre-existing ones[5–7]. It is interrelated to several physiological functions and also, it is a fundamental step in numerous diseases including cancer[8]. Furthermore, it has a significant role in tumour progression and development[9,10].

At present, there are main approaches in targeting angiogenesis that has been verified in clinical trials and officially approved in clinical practice[11]: i) monoclonal antibodies which bind to vascular endothelial growth factor-A (VEGF-A) e.g. bevacizumab[12]; ii) VEGF-trap e.g. aflibercept which binds to VEGF-A, VEGF-B, and placental growth factor (PGF)[13]; iii) monoclonal antibodies targeting VEGF receptors and block the binding of natural VEGFR ligands e.g. ramucirumab, iv) tyrosine kinase inhibitors (TKIs) which are drugs that inhibit the kinase activity of VEGF receptors through binding to the ATP binding site. Hence, TKIs hinder the phosphorylation of the tyrosine residue and subsequent transmission of signalling down the intercellular pathway. Among this class of agents, sorafenib **1** and sunitinib **2** are the prototypes[14]. There have been numerous known tyrosine kinase receptors such as vascular endothelial growth factor receptors (VEGFRs) and endothelial growth factor receptors (EGFRs)[15].

It has been stated that the vascular endothelial growth factor (VEGF) can stimulate the production and movement of vascular endothelial cells and regulate the formation of blood vessels[12,16]. There are three main vascular endothelial growth factor receptors (VEGFR-1, VEGFR-2, and VEGFR-3), which are strategic intermediates in angiogenesis and in the construction of new networks of blood vessels required to hoard oxygen and nourishment for cancer growth[17].

Vascular endothelial growth factor receptor-2 (VEGFR-2) is the most critical regulator of angiogenic factors that plays a significant role in tumour survival, angiogenesis, and migration[18]. Binding of VEGFR-2 to VEGF leads to inspiration of downstream signalling pathway and certain endothelial reactions, such as improved permeability of vascular cells and increased endothelial cell multiplying and propagation, consequently, lead to angiogenesis[19]. Hence,

CONTACT Hazem Elkady Hazemelkady@azhar.edu.eg Pharmaceutical Medicinal Chemistry & Drug Design Department, Faculty of Pharmacy (Boys), Al-Azhar University, Cairo 11884, Egypt; Nawaf A. Alsaif nalsaif@KSU.EDU.SA Department of Pharmaceutical Chemistry, College of Pharmacy, King Saud University, Riyadh, Saudi Arabia; Alaa Elwan alaaelwan34@azhar.edu.eg Pharmaceutical Medicinal Chemistry & Drug Design Department, Faculty of Pharmacy (Boys), Al-Azhar University, Cairo 11884, Egypt

Supplemental data for this article can be accessed here.

© 2021 The Author(s). Published by Informa UK Limited, trading as Taylor & Francis Group.
This is an Open Access article distributed under the terms of the Creative Commons Attribution License (http://creativecommons.org/licenses/by/4.0/), which permits unrestricted use, distribution, and reproduction in any medium, provided the original work is properly cited.

blockage of VEGF/VEGFR-2 system is considered a favourable approach for anti-angiogenic therapy in retarding cancer growth[20,21]. Additionally, VEGFR-2 has been confirmed to motivate apoptosis in cancer cells which synergistically enhances the antitumor effect[22–25].

Apoptosis has two major pathways; the intrinsic pathway which is controlled by the Bcl-2 family (involve BAX and Bcl-2) and the extrinsic pathway which is controlled by a subgroup of tumour necrosis factor receptors superfamily (TNFR)[26]. Immediately as the apoptosis process is instigated, caspases, a family of protease enzymes, are activated. Caspases are classified into initiator caspases as caspases 8 and 9, effector caspases as caspases 3, 6, and, 7 and inflammatory caspases as caspases 1, 4, 5, 11, and 12[26]. Caspase 9 is the initiator of intrinsic apoptosis while caspase 3 plays a central role in the execution phase of apoptosis[27]. Cancer cells can avoid apoptosis by hindering caspase function, decreasing BAX expression level or increasing the gene expression level of anti-apoptotic Bcl-2[27,28].

A literature study revealed that VEGFR-2 inhibitors have main pharmacophoric features[29–31]. (i) A flat heteroaromatic ring system that can accommodate the hinge region[29]. (ii) A central spacer moiety that can occupy the linker region between the hinge region and DFG domain of the enzyme[32]. (iii) A pharmacophore moiety consists of an H-bond acceptor (HBA) and an H-bond donor (HBD). Such pharmacophore moiety can interact with the two vital amino acid residues (Asp1044 and Glu883) in the DFG motif region[33]. (iv) A terminal hydrophobic moiety that occupies the allosteric hydrophobic pocket via numerous hydrophobic interactions[34] (Figure 1).

Also, a literature review revealed that many VEGFR-2 inhibitors have been approved as potent anticancer agents such as sorafenib **1**[35], Sunitinib **2**[36], lenvatinib **3**[37,38], lucitanib **4**[37,38], and fruquinitinib **5**[39]. All of them fulfilled the main pharmacophoric features of VEGFR-2 inhibitors (Figure 2).

1.1. Rationale of molecular design

Based on facts mentioned above and in the extension of our efforts to discover novel molecules with potential anticancer activity[5,40–48], we design and synthesise a new wave of bis([1, 2, 4]triazolo)[4,3-*a*:3′,4′-*c*]quinoxaline derivatives having the basic crucial pharmacophoric features of VEGFR-2 inhibitors.

At first, bis([1, 2, 4]triazolo)[4,3-*a*:3′,4′-*c*]quinoxaline moiety was selected as a heteroaromatic ring system to occupy the hinge region in the ATP binding site. Such moiety was accomplished to attain more rigid structures that could increase binding affinity against the active site. Then, sulfanyl-*N*-phenylacetamide moiety was utilised as a central spacer to occupy the linker region. Such spacer was expected to increase the flexibility of the designed compounds. Regarding the DFG-motif region, we used two different moieties having the essential HBA/HBD features to play the role of the pharmacophore. The pharmacophores were designed to be amide moiety (compounds **23a**–**n**), or diamide moiety (compounds **24a**–**c**). Finally, the allosteric hydrophobic region can be occupied by different terminal aliphatic moieties (**23a**–**f**) or terminal aromatic moieties (**23 g**–**n** and **24a**–**c**). These wide varieties of modifications helped us to study the SAR of these compounds as efficient anticancer agents with potential VEGFR-2 inhibitory activities. All modification pathways and molecular design rationale were illustrated and summarised in Figure 3. As shown in Figure 4, the target compounds achieved the essential pharmacophoric requirements of VEGFR-2 inhibitors.

To attain our aim of this work, cytotoxicity and VEGFR-2 inhibitory effects of the synthesised compounds were assessed. Besides, flow cytometric analyses were carried out for the most active candidate to estimate its potential against apoptosis induction and cell cycle arrest. Furthermore, such a compound was examined against several apoptotic markers include caspase 3/9 and BAX, and Bcl-2.

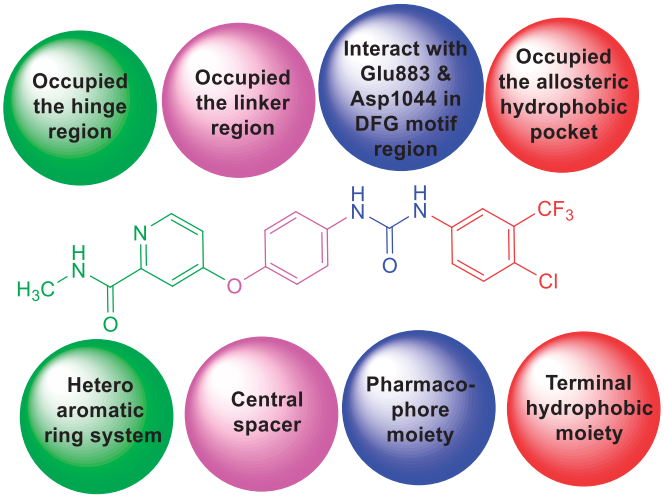

Figure 1. The essential structural requirements of reported VEGFR-2 inhibitors.

2. Results and discussion

2.1. Chemistry

The general synthetic pathways adopted for the synthesis of the designed compounds are illustrated in Schemes 1–3. Scheme 1 depicts the synthesis of potassium bis[1, 2, 4]triazolo[4,3-*a*]quinoxaline-4-thiolate **14**. Initially, *o*-phenylenediamine **6** was refluxed with oxalic acid **7** in the presence of 4 N HCl to afford 2,3-(1*H*,4*H*)-quinoxalinedione **8**[49]. Chlorination of compound **8** was done by refluxing with thionyl chloride yielding 2,3- dichloroquinoxaline **9**[49]. Subsequent treatment of the latter with hydrazine hydrate in absolute ethanol afforded 2-chloro-3-hydrazinylquinoxaline **10**[50]. Heating of compound **10** with triethyl orthoformate gave 4-chloro[1, 2, 4]triazolo[4,3-*a*]quinoxaline **11**[50]. The obtained compound **11** was heated with hydrazine hydrate to afford 4-hydrazinyl-[1, 2, 4] triazolo[4,3-*a*]quinoxaline **12**[51]. Moreover, reflux of **12** in an alcoholic mixture of carbon disulphide and potassium hydroxide afforded bis[1, 2, 4]triazolo[4,3-*a*:3′,4′-*c*]quinoxaline-3-thiol **13**[44]. Heating compound **13** with an alcoholic solution of potassium hydroxide gave the corresponding potassium salt **14**[44]. (Scheme 1)

Scheme 2 was carried out to prepare the key intermediates (**18a**–**n** and **22a**–**c**). At first, acetylation of *p*-amino benzoic acid **15** with chloroacetyl chloride in DMF in the presence of $NaHCO_3$ provided the key product 4–(2-chloroacetamido)benzoic acid **16**. Compound **16** was acylated using thionyl chloride to produce the benzoyl chloride derivative **17**[52]. Furthermore, stirring of compound **17** with commercially available amines namely, ethylamine, *n*-butylamine, *sec*-butylamine, *tert*- butylamine, cyclopentylamine, cyclohexylamine, 4-aminoacetophenone, 3-chloroaniline, 4-chloroaniline, 2,5-dichloroaniline, 4-fluoroaniline, 2-hydroxyaniline, 4-hydroxyaniline, and 2-hydroxy-4-nitroaniline at room temperature in acetonitrile/TEA mixture afforded the corresponding intermediates **18a**–**n**, respectively. On the other hand, to prepare the ester derivatives **20a**–**c,** appropriate acid derivatives **19a**–**c** namely, 2-chlorobenzoic acid, 3-chlorobenzoic, and 2-hydroxybenzoic acid

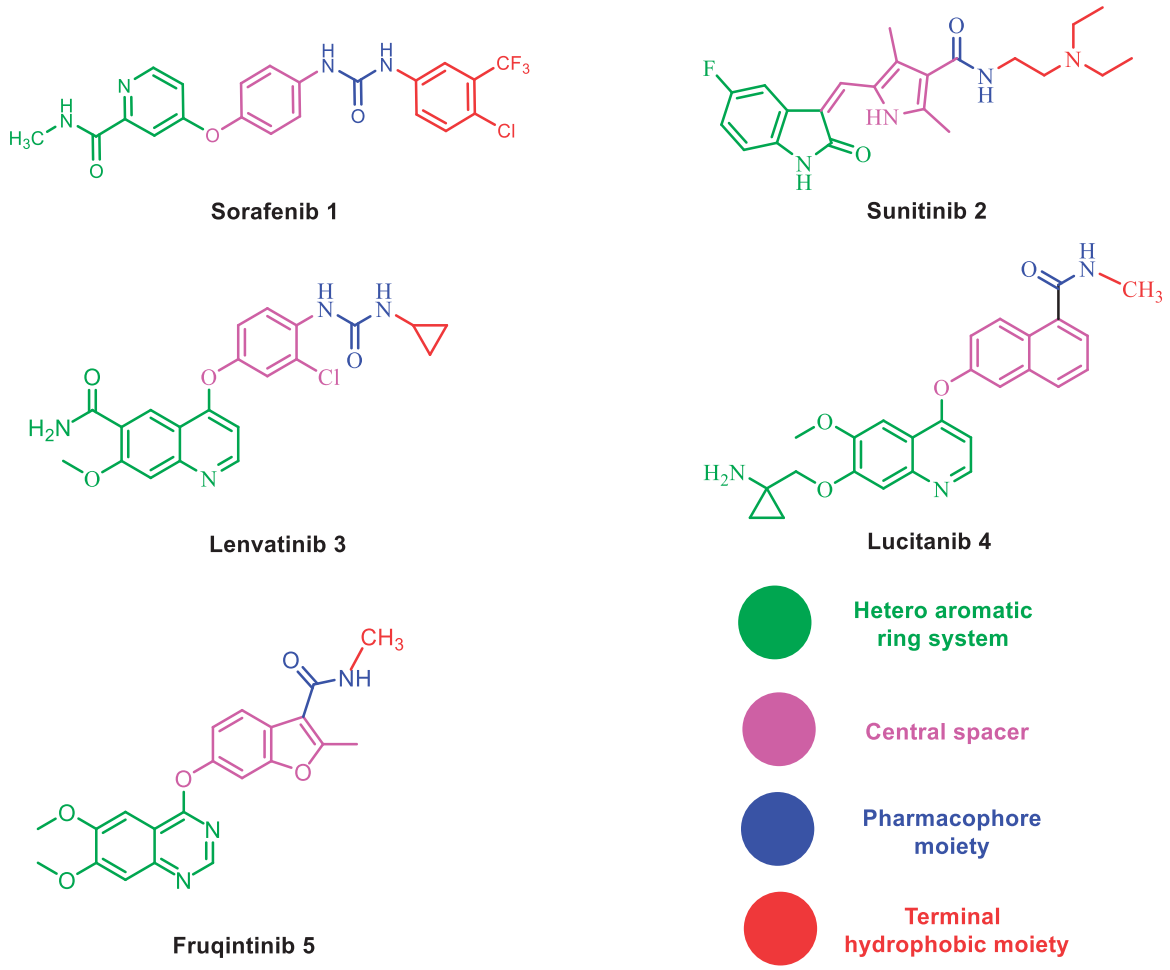

Figure 2. Structures of some representative VEGFR-2 inhibitors.

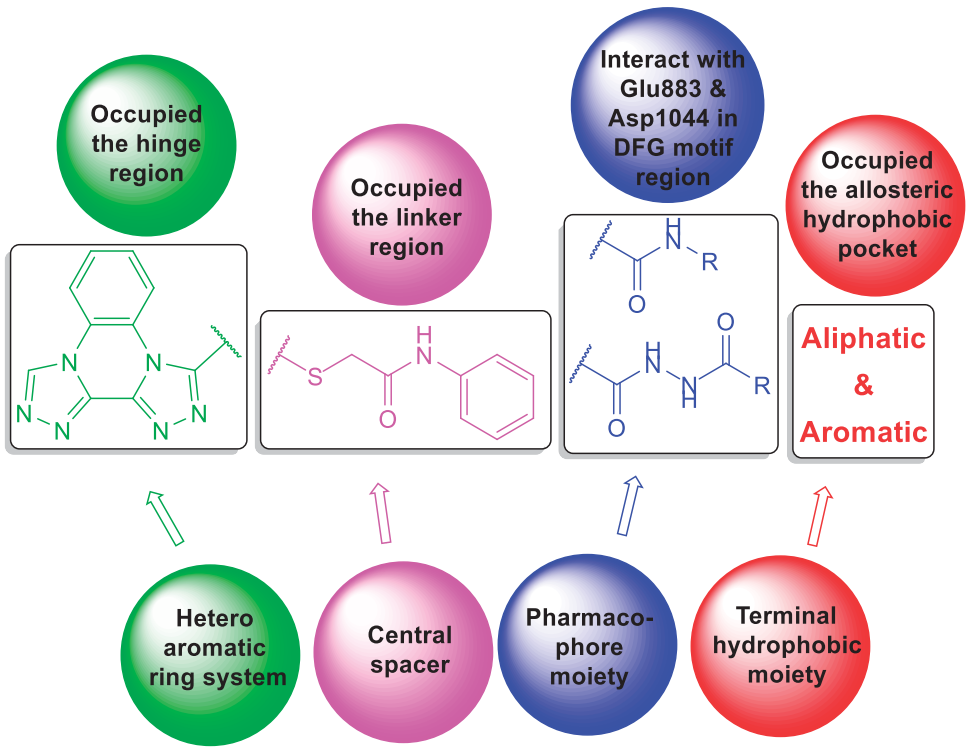

Figure 3. Schematic representation showing the designing strategy.

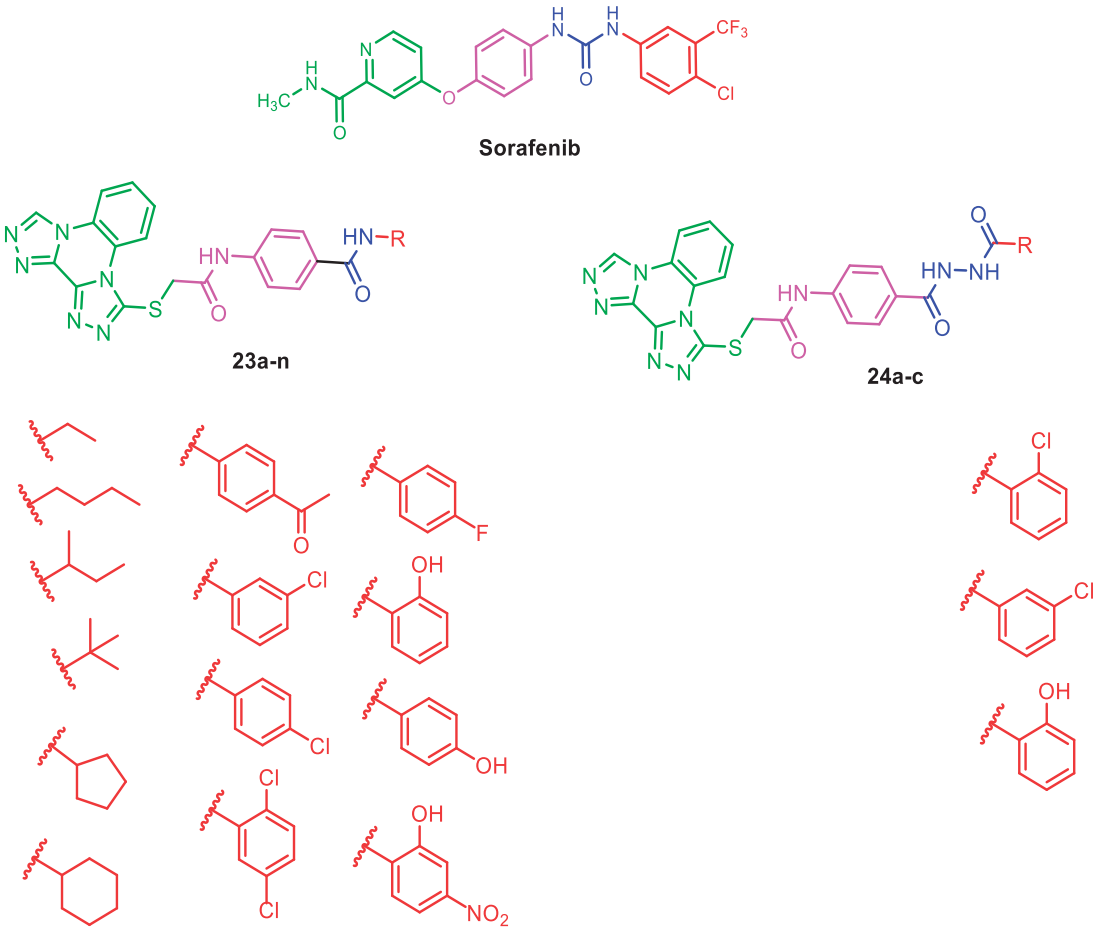

Figure 4. The target compounds fulfilled the pharmacophoric features of VEGFR-2 inhibitors.

were refluxed in methanol in the presence of sulphuric acid according to the reported procedures[42,53,54]. In addition, reflux of **20a**–**c** with hydrazine hydrate afforded the corresponding acid hydrazides **21a**–**c**[42]. In the end, in acetonitrile and TEA mixture, compound **17** was stirred with the acid hydrazides **21a**–**c** to produce the corresponding diamide derivatives **22a**–c (Scheme 2).

The structures of compounds **18a**–**n** and **22a**–**c** were confirmed by spectral and elemental data. IR spectra of such compounds showed strong bands around $3370-3100\,cm^{-1}$ corresponding to NHs. Also, IR spectra showed strong C=O absorption bands at a range of $1770-1624\,cm^{-1}$. Moreover, ^{1}H NMR spectra showed singlet signals around δ 10.50 and 8.35 ppm corresponding to the two amidic NHs. Additionally, CH_2 protons appeared at around δ 4.30 ppm. Matching with such results, ^{13}C NMR spectra also confirmed the validity of suggested structures where characteristic peaks were displayed around δ 165.60, 165.05, and 44.00 ppm corresponding to the two C=O and CH_2 groups, respectively.

Scheme 3 demonstrated the synthetic pathway of the final target compounds (**23a**–**n** and **24a**–**c**). Compound **14** was heated with the formerly synthesised intermediates (**18a**–**n** and **22a**–**c**) in dry DMF using KI to furnish the titled compounds **23a**–**n** and **24a**–**c**, respectively.

The spectral and elemental data supported the structures of the obtained derivatives, where the ^{1}H NMR spectra of compounds **23a**–**n** and **24a**–**c** displayed characteristic downfield singlet signals around δ 10.75 ppm. The mass spectra were also consistent with the expected structures. Taking compound **23d** as a representative example, the IR spectrum demonstrated stretching bands at 2968 and $2929\,cm^{-1}$ corresponding to aliphatic CH bonds. The ^{1}H NMR spectrum of this compound showed an up-field singlet signal at δ 1.38 ppm corresponding to tertiary butyl moiety. Furthermore, ^{13}C NMR spectrum showed the presence of two peaks at δ 51.16 and 29.11 corresponding to CH and three CH_3 of *tert*-butyl moiety.

2.2. Biological evaluation

2.2.1. In vitro *anti-proliferative activity*

All newly prepared compounds were assessed for their *in vitro* cytotoxic efficiencies via standard MTT method[55–57], against breast cancer (MCF-7) and hepatocellular carcinoma (HepG2) cell lines. Sorafenib was applied as a standard anticancer drug. The growth inhibitory concentration (IC_{50}) values were concluded for each final compound and depicted in Table 1.

Overall, HepG2 cells were more sensitive to the tested compounds than MCF-7 except for compound **23k**. Among the series, compound **23j** showed the highest anti-proliferative activities against MCF-7 and HepG2 cell lines with IC_{50} values of 10.3 and 6.4 μM, respectively. In addition, compounds **23a**, **23i**, **23 l**, and **23n** exhibited good anti-proliferative activities against the tested cell lines with IC_{50} values ranging from 7.1 to 19.4 μM, comparing to sorafenib (IC_{50} = 3.51 and 2.17 μM against MCF-7 and HepG2, respectively). Moreover, compounds **23d**, **23h**, **23m**, **24a**, **24b**, and **24c** displayed moderate anti-proliferative activities against the tested cell lines with IC_{50} values ranging from 15.2 to 48.3 μM. On the other hand, the rest of the compounds displayed weak anti-proliferative activities against the tested cell lines.

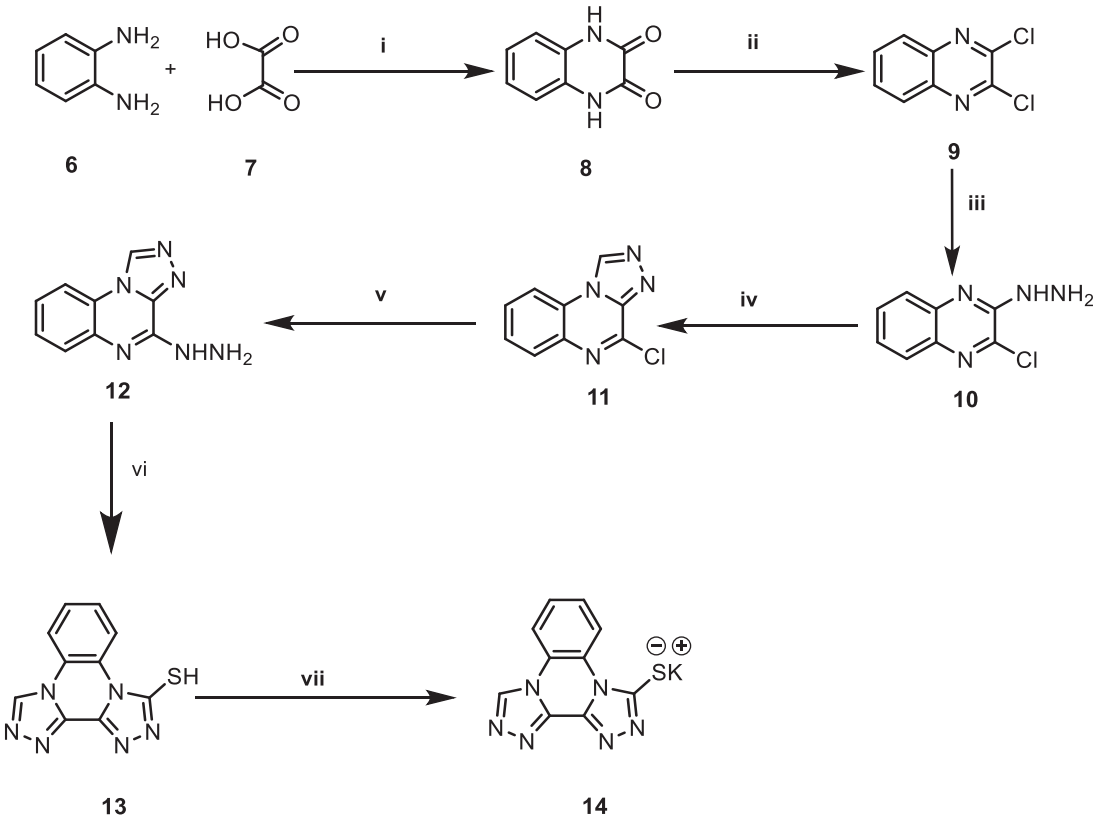

Scheme 1. Synthetic pathway for compound **14**; Reagents and conditions: (i) 4 N conc. HCl/reflux/6 h, (ii) $SOCl_2$/DCE/reflux/4 h, (iii) $NH_2NH_2.H_2O$/ethanol/r.t., (iv) triethyl orthoformate/reflux/4 h, (v) $NH_2NH_2.H_2O$/ethanol/reflux/4 h, (vi) absolute ethanol/KOH/CS_2/reflux/6 h, (vii) absolute ethanol/KOH/heating/10 min.

2.2.2. In vitro *VEGFR-2 enzyme assay inhibition*

All the synthesised compounds were subjected to further assay for their ability to inhibit VEGFR-2 using sorafenib as a positive control. The results were stated as growth inhibitory concentration (IC_{50}) values and illuminated in Table 1.

Compound **23j** was the most potent VEGFR-2 inhibitor with an IC_{50} value of 3.7 nM, nearly equal to that of sorafenib (IC_{50} = 3.12 nM). Moreover, compounds **23a**, **23d**, **23h**, **23i**, **23l**, **23m**, and **23n** showed promising activities with IC_{50} values ranging from 5.8 to 11.8 nM. On the other hand, compounds **23c**, **23e**, **23f**, **23k**, and **24a–c** exhibited moderate to weak activity with IC_{50} values ranging from 20.7 to 49.6 nM. Finally, compounds **23b** and **23g** exhibited the lowest anti VEGFR-2 activities with IC_{50} values of 71.6 and 62.7 nM, respectively.

2.2.3. *Structure–activity relationship (SAR)*

Inspecting the results of different biological analyses (anti-proliferative activity and VEGFR-2 assay); we concluded a valuable SAR.

At First, the effect of pharmacophore moiety on the activity was explored. It was noticed that the amide derivatives **23h** (IC_{50} = 37.2 and 22.3 μM against MCF-7 and HepG2, respectively & 11.7 nM against VEGFR-2) and **23 l** (IC_{50} = 19.4 and 11.3 μM against MCF-7 and HepG2, respectively & 5.8 nM against VEGFR-2) displayed higher activities than the corresponding diamide derivatives **24b** (IC_{50} = 42.7 and 30.3 μM against MCF-7 and HepG2, respectively & 22.3 nM against VEGFR-2) and **24c** (IC_{50} = 40.7 and 29.8 μM against MCF-7 and HepG2, respectively & 20.7 nM against VEGFR-2).

Next, we investigated the effect of the terminal hydrophobic moiety. With respect to the terminal aliphatic hydrophobic moieties, it was found that the VEGFR-2 inhibitory activities decreased in the order of ethyl (**23a**, IC_{50} = 7.1 nM) > *tert*-butyl (**23d**, IC_{50} = 11.8 nM) > cyclohexyl (**23f**, IC_{50} = 39.5 nM) > cyclopentyl (**23e**, IC_{50} = 39.8 nM) > *sec*-butyl (**23c**, IC_{50} = 47.1 nM) > *n*-butyl (**23b**, IC_{50} = 71.6 nM). In addition, the effect of the substitution on the aromatic hydrophobic moieties has been examined. For the amide derivatives, it was found that the VEGFR-2 inhibitory activities decreased in the order of 2,5-dichloro (**23j**, IC_{50} = 3.7 nM) >2-hydroxy (**23l**, IC_{50} = 5.8 nM) >2-hydroxy −4-nitro (**23n**, IC_{50} = 7.4 nM) >4-chloro (**23i**, IC_{50} = 9.4 nM) >4-hydroxy (**23m**, IC_{50} = 9.7 nM) >4-fluoro (**23k**, IC_{50} = 49.6 nM). While the diamide derivatives revealed decrease in VEGFR-2 inhibitory activities in the order of 2- hydroxy (**24c**, IC_{50} = 20.7 nM) >3-chloro (**24b**, IC_{50} = 22.3 nM) > 2-chloro (**24a**, IC_{50} = 23.9 nM).

2.2.4. *Correlation of cytotoxicity with VEGFR-2 inhibition*

From the aforementioned results, we can conclude that our tested compounds can inhibit VEGFR-2 in the tested cell lines. To prove that inhibition of VEGFR-2 is the major prominent cause of cell mortality, we compared the cytotoxicity results of the synthesised candidates with their corresponding VEGFR-2 inhibitory activities utilising a simple linear regression analysis. The coefficients of determination (R^2) were determined. The R^2 values for MCF-7 and HepG2 were 0.881 (*p* values >.0001) and 0.800 (*p* values > .0001), respectively (Figure 5). Such high values of R^2 indicate the high correlation between the dependent variable (VEGFR-2 inhibition) and the independent one (cytotoxicity).

2.2.5. *Cellular mechanistic study*

Compound **23j** which demonstrated remarkable cytotoxic potency and significant inhibitory activity against VEGFR-2 was nominated

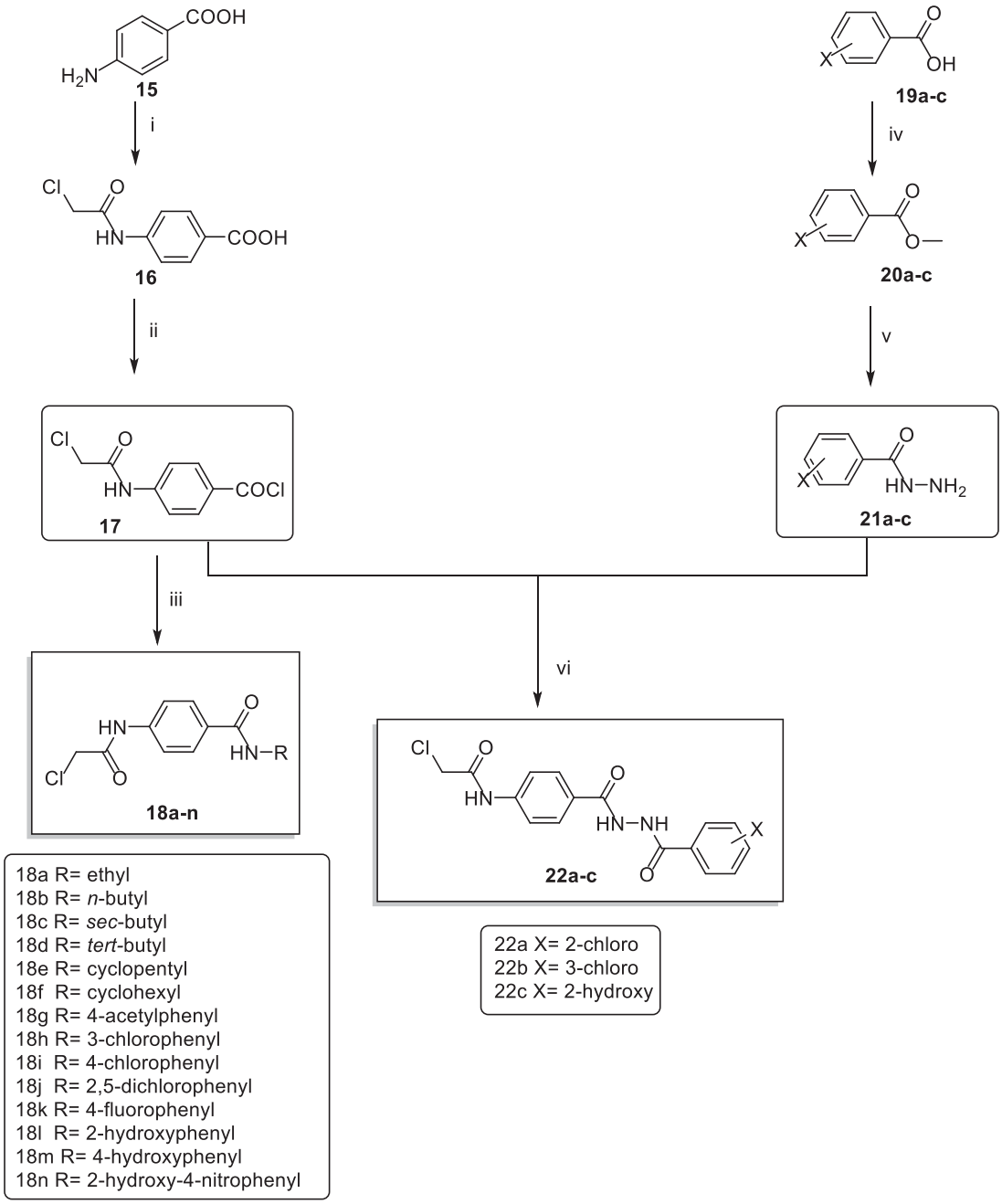

Scheme 2. Synthetic pathway for compounds **18a**–**n** and **22a**–**c**; Reagents and conditions: (i) $ClCH_2COCl$/DMF/$NaHCO_3$/r.t./1 h, (ii) $SOCl_2$/DCE/DMF/reflux/4 h, (iii) RNH_2/acetonitrile/TEA/r.t./8 h (iv) methanol/conc.H_2SO_4/reflux/8 h, (v) $NH_2NH_2.H_2O$/ethanol/reflux/8 h, (vi) acetonitrile/TEA/r.t./8 h.

for further cellular mechanistic study. This involved study of its influence on cell cycle progression and induction of apoptosis in HepG2 cells.

2.2.5.1. Effect on cell cycle progression. In this work, HepG2 cell line was treated with compound **23j** at a concentration of 6.4 μM (the IC_{50} value of compound **23j**) and incubated for 24 h. Then, the cells were stained with propidium iodide and analysed for cell distribution during the various phases of the cell cycle against untreated HepG2 cells. Flow cytometry results exhibited that the percent of HepG2 cells decreased at the Sub-G1, G1 and S phases. For Sub-G1 phase, it decreased from 1.46% to 1.21%, for G1 phase it decreased from 57.75 to 37.34% while for S phase it decreased from 28.65% to 25.79%. On the other hand, the percentage of HepG2 cells significantly increased at G2/M phase from 12.13% to 35.64%. Such results indicated that compound **23j** inhibited proliferation of HepG2 cells via cessation of the growth of the cell cycle at G2/M phase (Table 2 and Figure 6).

2.2.5.2. Apoptosis analysis. To confirm the apoptotic ability of compound **23j**, a flow cytometry technique was performed. In such technique, HepG2 cells were stained with annexin V/propidium iodide (PI) and incubated for 24 h with compound **23j** (6.4 μM). It was revealed that compound **23j** triggered more apoptotic cells comparing to untreated control cells. In details, compound **23j** induced apoptosis by 40.12% (early apoptosis = 39.97% & late apoptosis = 0.15%), compared to 7.07% in the control cells (early apoptosis = 6.88% & late apoptosis = 0.19%).

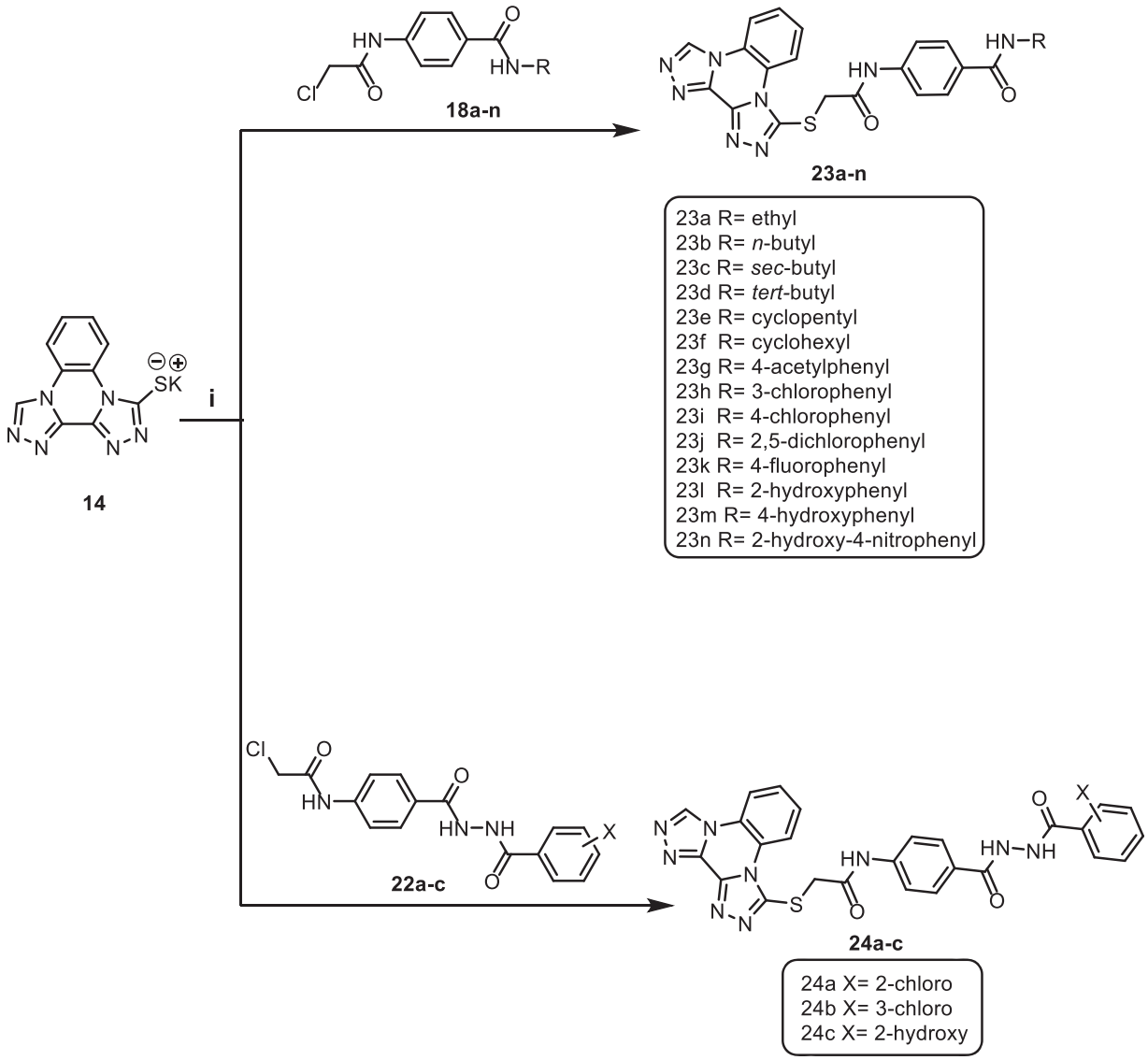

Scheme 3. Synthetic pathway for compounds **23a–n** and **24a–c**; Reagents and conditions: (i) DMF/KI/reflux/6 h.

Table 1. *In vitro* anti-proliferative activities of the tested compounds against MCF-7 and HepG2 cell lines, and *in vitro* enzymatic inhibitory activities against VEGFR-2.

Comp.	IC_{50} (μM)[a] MCF-7	IC_{50} (μM)[a] HepG2	IC_{50} (nM)[a] VEGFR-2
23a	17.7 ± 1.5	11.3 ± 0.9	7.1 ± 0.4
23b	78.9 ± 6.1	69.1 ± 6.1	71.6 ± 5.2
23c	76.2 ± 6.9	69.8 ± 5.9	47.1 ± 4.2
23d	21.6 ± 1.8	17.5 ± 1.2	11.8 ± 0.8
23e	78.3 ± 6.5	74.8 ± 6.9	39.8 ± 3.1
23f	74.1 ± 6.7	70.4 ± 5.8	39.5 ± 2.9
23g	81.3 ± 7.4	80.7 ± 7.1	62.7 ± 5.7
23h	37.2 ± 3.2	22.3 ± 1.8	11.7 ± 0.9
23i	18.3 ± 1.2	10.8 ± 0.9	9.4 ± 0.7
23j	10.3 ± 0.8	6.4 ± 0.5	3.7 ± 0.2
23k	68.2 ± 5.2	71.8 ± 6.3	49.6 ± 4.1
23l	19.4 ± 1.1	11.3 ± 0.7	5.8 ± 0.3
23m	21.6 ± 1.7	15.2 ± 1.2	9.7 ± 0.7
23n	16.5 ± 1.3	12.7 ± 0.9	7.4 ± 0.5
24a	48.3 ± 3.9	34.5 ± 2.8	23.9 ± 1.9
24b	42.7 ± 3.7	30.3 ± 2.7	22.3 ± 1.8
24c	40.7 ± 3.7	29.8 ± 2.1	20.7 ± 1.6
Sorafenib	3.51 ± 0.22	2.17 ± 0.14	3.12 ± 0.1

[a]IC_{50} values are the mean ± SD of three separate experiments.

Such findings revealed that compound **23j** could induce apoptosis in HepG2 cells (Table 3 & Figure 7).

2.2.5.3. Caspase 3/9 assay. To study the effect of compound **23j**, the most promising member, on caspase-3 and caspase-9 levels, western blot technique was carried out. HepG2 cells were treated with **23j** (6.4 μM) for 24 h. The results revealed that compound **23j** produced a significant increase in the cellular levels of caspase-3 (1.36-fold) and caspase-9 (2.80-fold) compared to the control cells (Table 4 and Figure 8).

2.2.5.4. Evaluation of BAX and Bcl-2 expressions. BAX and Bcl-2 cellular levels were assessed for compound **23j** after 24 h of its application on HepG2 cells using western blot technique. The results showed that compound **23j** produced an increase of the pro-apoptotic factor BAX by 1.65-fold while anti-apoptotic protein Bcl-2 demonstrated a concentration decreased by 2.63-fold. Moreover, compound **23j** increased BAX/Bcl-2 ratio to be 4.34 which indicates the efficiency of compound **23j** on apoptosis cascade (Table 4 and Figure 8).

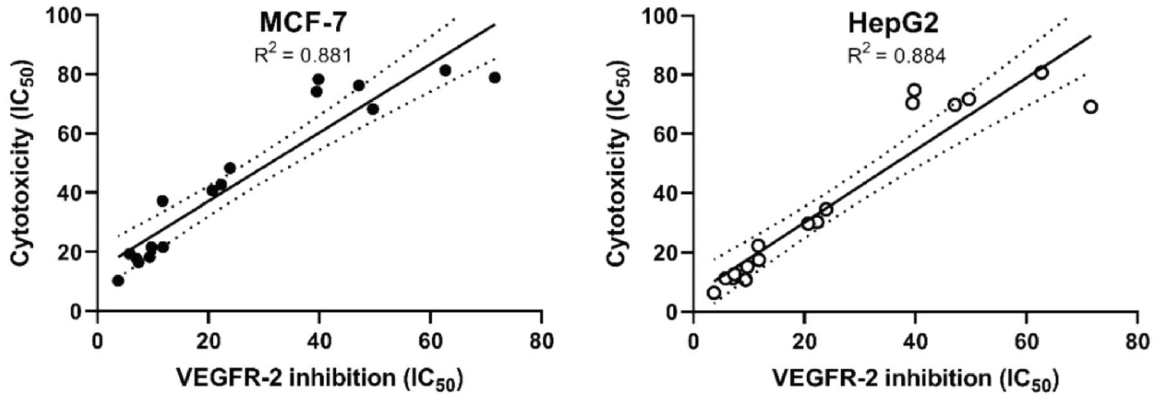

Figure 5. Correlation of cytotoxicity with VEGFR2 inhibition on two cell line models MCF-7and HepG2. MCF-7 (p value >.0001) & HepG2 (p value >.0001).

Table 2. Effect of compound **23j** on cell cycle progression in HepG2 cells after 24 h treatment.

	Cell cycle distribution (%)[a]			
Sample	%Sub-G1	%G1	%S	%G2 / M
HepG2	1.46 ± 0.17	57.75 ± 2.34	28.65 ± 2.74	12.13 ± 0.80
Compound **23j/HepG2**	1.21 ± 0.15	37.34 ± 2.50**	25.79 ± 1.21	35.64 ± 2.16***

[a]Values are given as mean ± SEM of three independent experiments. **$p < .01$ and ***$p < .001$.

2.3. Molecular modelling study

2.3.1. Docking study

Molecular docking study was accomplished to get further insight into the binding modes and orientations of the newly synthesised compounds into the ATP binding site of VEGFR-2 enzyme. Sorafenib was used as a reference ligand. Validation of the docking procedure was achieved via re-docking of the co-crystallised ligand against the active pocket of VEGFR-2. The results revealed that the RMSD value between the re-docked pose and the co-crystallised one was 1.02. This value revealed the validity of the docking process (Figure 9). The calculated ΔG (binding free energies) of the synthesised compounds and the reference drug against VEGFR-2 were summarised in Table 5.

Sorafenib interactions with the amino acids of the active site have been studied and displayed in 2 D and 3 D style in Figure 10. The proposed binding mode of sorafenib revealed an affinity value of −22.48 kcal/mol. The *N*-methylpicolinamide moiety formed five hydrophobic interactions with Val846, Ala864, Phe1045, Leu1033, and Leu838. Likewise, it formed one hydrogen bond with Cys917. Moreover, the phenyl moiety was buried in the linker region forming five hydrophobic interactions with Phe1045, Cys1043, Val846, Val914, and Val897. Furthermore, the pharmacophore moiety (urea group) formed three hydrogen bonds with the two crucial amino acids Glu883 and Asp1044. Finally, the 1-chloro-2-(trifluoromethyl)benzene moiety conquered the allosteric hydrophobic region forming many hydrophobic and electrostatic interactions with Ile886, Leu887 Leu1017, His1024, Ile890, and Asp1044[34,58].

Docking simulation of compound **23i** revealed that it has a good fitting into the enzyme active sites with docking score of −23.63 kcal/mol. In DFG region, the amide moiety (pharmacophore) formed two hydrogen bonds with carboxylate moiety of Glu883 (1.50 Å) and NH group of Asp1044 (1.82 Å). Furthermore, the phenyl ring (central spacer) occupied the linker region forming five hydrophobic interactions with Cys1043, Phe1045, Val897, and Val914. Also, the bis([1, 2, 4]triazolo)[4,3-*a*:3′,4′-*c*]quinoxaline moiety occupied the hinge region forming two hydrophobic and one hydrogen bond interactions with Leu838. Additionally, the terminal hydrophobic (4-chlorophenyl) moiety formed three hydrophobic interactions with Ile886 and Leu887 and one electrostatic interaction with Asp1044 (Figure 11).

The docking findings of compound **23j** revealed affinity value of −23.87 kcal/mol. The amide moiety formed two hydrogen bonds with Glu883 (COO^-, 1.75 Å) and Asp1044 (NH, 2.20 Å). Additionally, in the hinge region, the docked compound formed four hydrophobic interactions via its bis([1, 2, 4]triazolo)[4,3-*a*:3′,4′-*c*]quinoxaline moiety with Leu838 and Phe916. Also, the central phenyl ring moiety formed three hydrophobic interactions with Val914, Val897, and Cys1043. Finally, the 2,5-dichlorophenyl moiety formed electrostatic and hydrophobic interactions with Asp1044, Ile890, and Leu 887 (Figure 12).

Compound **23l** (affinity value of −23.26 kcal/mol) combined with the receptor protein as follows; In DFG domain, the amide moiety formed two hydrogen bonds with Glu883 (distance: 2.28 Å) and Asp1044 (distance: 1.76 Å). Moreover, in the hinge region, bis([1, 2, 4]triazolo)[4,3-*a*:3′,4′-*c*]quinoxaline moiety formed three hydrophobic interactions with His814 and Ile886. Also, in the linker region, the central phenyl ring moiety formed two hydrophobic interactions with Asp1044 and Leu887. Additionally, the terminal hydrophobic (2-hydroxyphenyl moiety) formed three hydrophobic interactions with Val897, Val914, and Lys866 (Figure 13).

2.3.2. In silico *ADME analysis*

To investigate pharmacokinetics properties of the prepared compounds, computer aided ADME studies were accomplished using Accelrys Discovery Studio 4.0 software. Sorafenib was used as a reference molecule. These studies include the estimation of certain parameters. 1) Blood brain barrier penetration which measures the ability of molecule to diffuse through blood brain barrier. 2) Absorption level which determines human intestinal absorption (HIA) of a chemical after its oral administration. A well-absorbed compound is one that is absorbed at least 90% into the blood stream[59,60]. iii) Solubility level in which the solubility of a chemical in water was predicted at 25 °C. iv) CYP2D6 binding which analyzes cytochrome P450 2D6 enzyme inhibition[61,62]. v) Plasma protein binding which predicts the fraction of drug bound to plasma proteins in the blood[63]. The results were predicted and listed in Table 6.

The results revealed that the estimated compounds have very low BBB penetration levels.

Accordingly, the CNS side effects of all compounds were expected to be low. Regarding absorption levels, compound **23a**

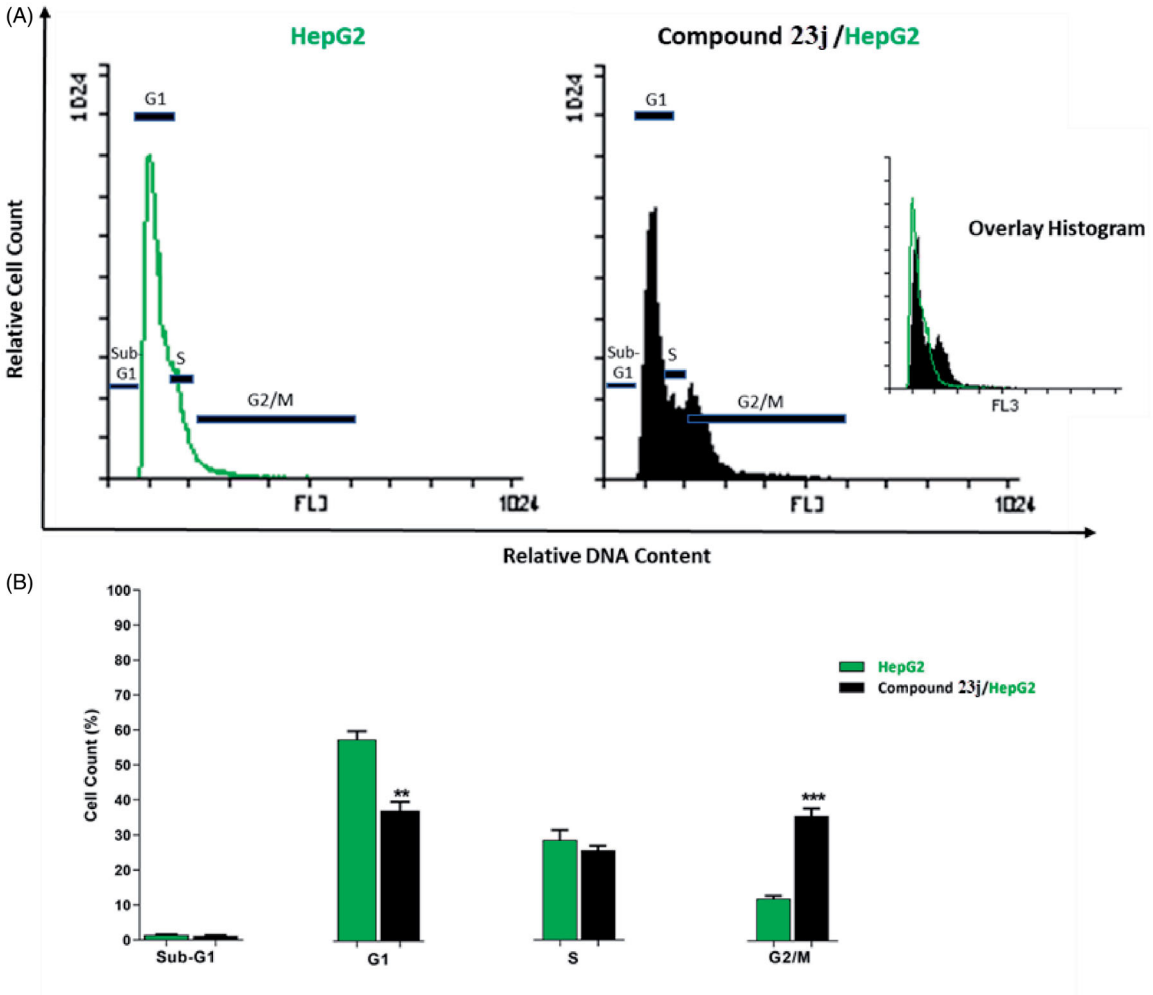

Figure 6. Cell cycle analysis of HepG2 cells treated with compound **23j**. $^{**}p < .01$ and $^{***}p < .001$.

Table 3. apoptotic effect of compound **23j** against HepG2 cells.

		Apoptosis[a]		
Sample	Viable[a] (left bottom)	Early (right bottom)	Late (right top)	Necrosis[a] (left top)
HepG2	92.80 ± 1.91	6.88 ± 0.90	0.19 ± 0.01	0.14 ± 0.01
Compound **23j/HepG2**	59.61 ± 2.88	39.97 ± 2.93***	0.15 ± 0.01	0.24 ± 0.07

[a]Values are given as mean ± SEM of three independent experiments. $^{***}p < .001$.

demonstrated good absorption level, compounds **23b**–**e** and **23k** exhibited moderate absorption levels. On the other hand, compounds **23f**–**j**, **23l**–**n**, and **24a**–**c** showed poor and very poor intestinal absorption. With respect to aqueous solubility, all compounds demonstrated low and very low levels of aqueous solubility. Moreover, the effect on cytochrome P450 2D6 was investigated. The results showed that all examined members were non-inhibitors of CYP2D6. Consequently, liver side effect is not expected upon their administration. The plasma protein binding model exhibited that all compounds were anticipated to bind plasma protein less than 90% (Figure 14).

2.3.3. Toxicity studies

Toxicity profile of the prepared candidates was assessed as stated by the validated and constructed models in Discovery studio software version 4.0[64,65]. These models involve: 1) FDA rodent carcinogenicity. 2) Carcinogenic potency TD_{50}[66]. 3) Rat maximum tolerated dose[67,68]. 4) Developmental toxicity potential[69,70]. 5) Rat oral LD_{50}[71]. 6) Rat chronic LOAEL[72,73].

Regarding FDA rodent carcinogenicity model, all the tested candidates were forecasted to be non-carcinogenic. For carcinogenic potency TD_{50} rat model, compounds **23a**,**b**, **23 l**,**m**, and **24c** showed TD_{50} values ranging from 33.907 to 44.001 g/kg body weight, which are higher than sorafenib (14.244). With respect to rat maximum tolerated dose model, compounds **23a**–**c**, **23 h**–**n**, and **24a**–**c** demonstrated maximum tolerated dose with a range of 0.099 to 0.391 g/kg body weight which are higher than that of sorafenib (0.089 g/kg body weight). On the other hand, compounds **23d**–**g** showed a maximum tolerated dose lower than that of sorafenib with a range of 0.083 to 0.088 g/kg body weight. Additionally, all compounds were predicted to be non-toxic against developmental toxicity potential model. For rat oral LD_{50} model, compounds **23a**–**d**, **23g**, **23i**, **23m**, and **24a**–**c** revealed oral LD_{50} values in a range of 0.864 to 2.477 g/kg body weight which are higher than that of sorafenib (0.823 g/kg body weight). For rat chronic LOAEL model, the tested compounds exhibited

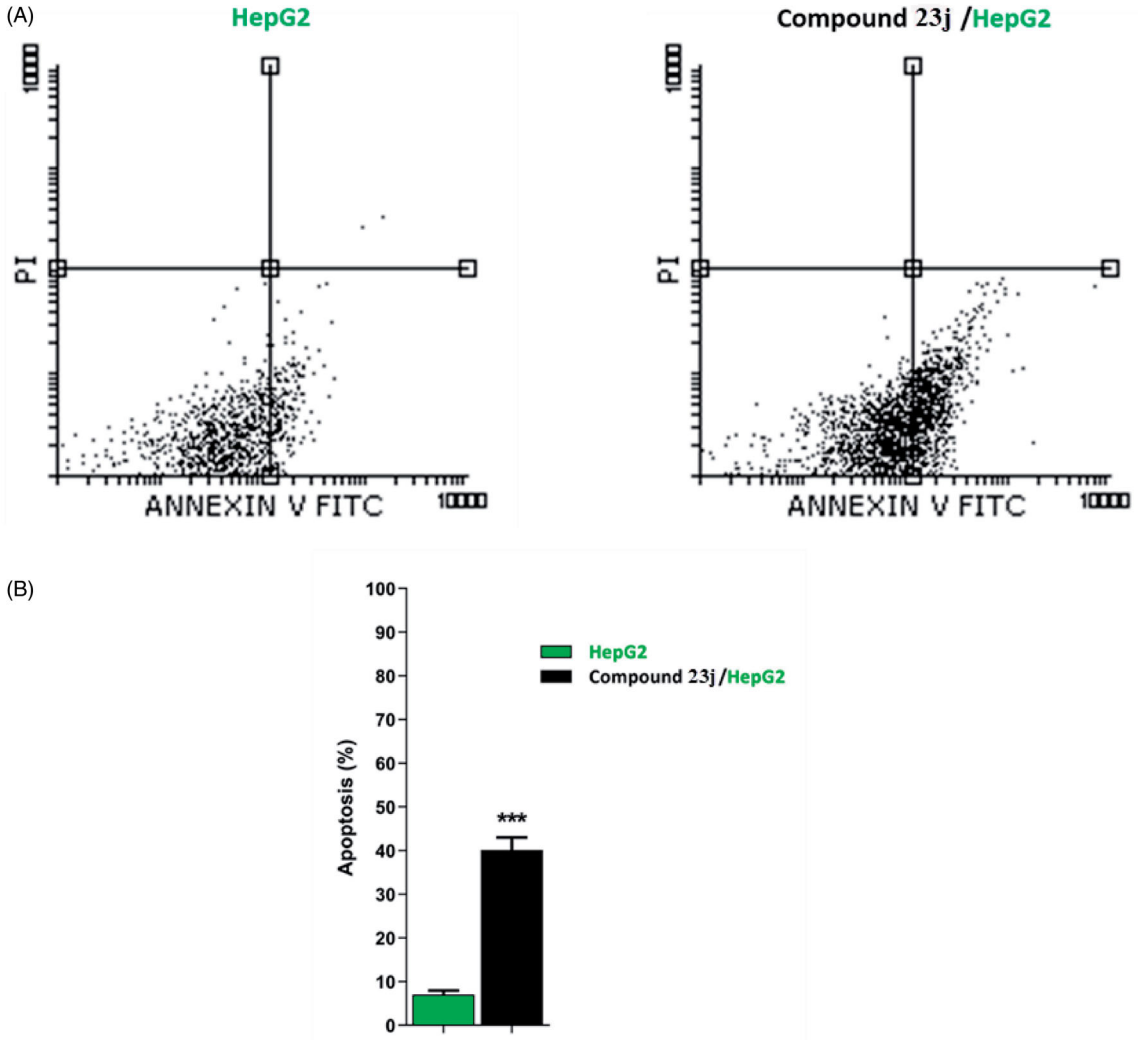

Figure 7. Flow cytometric analysis of apoptosis in HepG2 cells exposed to compound **23j**. $^{***}p < .001$.

Table 4. Effect of compound **23j** on levels of BAX, Bcl-2, active caspase-9, and active caspase-3 proteins expression

	Protein expression (normalized to β-actin)[a]				
Sample	BAX	Bcl-2	BAX/Bcl-2 ratio	Caspases-9	Caspases-3
HepG2	1.00 ± 0.13	1.00 ± 0.07	1.00 ± 0.10	1.00 ± 0.08	1.00 ± 0.03
23j/HepG2	1.65 ± 0.06*	0.38 ± 0.03**	4.34 ± 0.22***	2.80 ± 0.25**	1.36 ± 0.10*

[a]Values are given as mean ± SEM of three independent experiments. $^{*}p < .05$, $^{**}p < .01$ and $^{***}p < .001$.

LOAEL values ranging from 0.064 to 0.329 g/kg body weight. These values are higher than sorafenib (0.005 g/kg body weight) Table 7.

3. Conclusion

In the present study, a new series of bis([1, 2, 4]triazolo)[4,3-*a*:3′,4′-*c*]quinoxaline derivatives were synthesised as potential cytotoxic agents and VEGFR-2 inhibitors. The anticancer efficiency of these derivatives was evaluated against MCF-7 and HepG2 cancer cell lines. Four compounds **23a** (IC_{50} = 17.7 and 11.3 μM), **23i** (IC_{50} = 18.3 and 10.8 μM), **23j** (IC_{50} = 10.3 and 6.4 μM), **23l** (IC_{50} = 19.4 and 11.3 μM), and **23n** (IC_{50} =16.5 and 12.7 μM) were the most active antiproliferative members against MCF-7 and HepG2, respectively. The *in vitro* VEGFR-2 assay revealed that compounds **23a**, **23d**, **23h**, **23i**, **23j**, **23l**, **23m**, and **23n** exhibited the highest inhibitory activity versus VEGFR-2 with IC_{50} values of 7.1, 11.8, 11.7, 9.4, 3.7, 5.8, 9.7, and 7.4 nM, respectively. SAR revealed that the amide derivatives (compounds **23h** and **23l**) exhibited higher activities than the corresponding diamide derivatives (compounds **24b** and **24c**). Furthermore, compound **23j**, the most potent member, arrested the HepG2 cell growth at G2/M phase and induced apoptosis by 40.12% compared to the control cells (7.07%). Moreover, caspase activation assay was performed for **23j** in HepG2 cell lines. The results showed significant increase of caspase 3 (1.36-fold) and caspase 9 (2.80-fold). BAX and Bcl-2 concentration levels were also evaluated and showed a titre increase of the pro-apoptotic protein BAX (1.65-fold) and a decrease of Bcl-2 (2.63-fold). Additionally, compound **23j** increased BAX/Bcl-2 ratio to be 4.34. Finally, computational physicochemical assessment of the synthesised compounds showed that they have favourable properties with satisfactory drug-like profiles.

4. Experimental

4.1. Chemistry

All the reagents, chemicals, and apparatus were presented in Supplementary data. Compounds **8**, **9**, **10**, **11**, **12**, **13**, **14**, **16**, **17**, **20a**–**c**, and **21a**–**c** were prepared in accordance with the reported procedures[41,42,44,49,50,52].

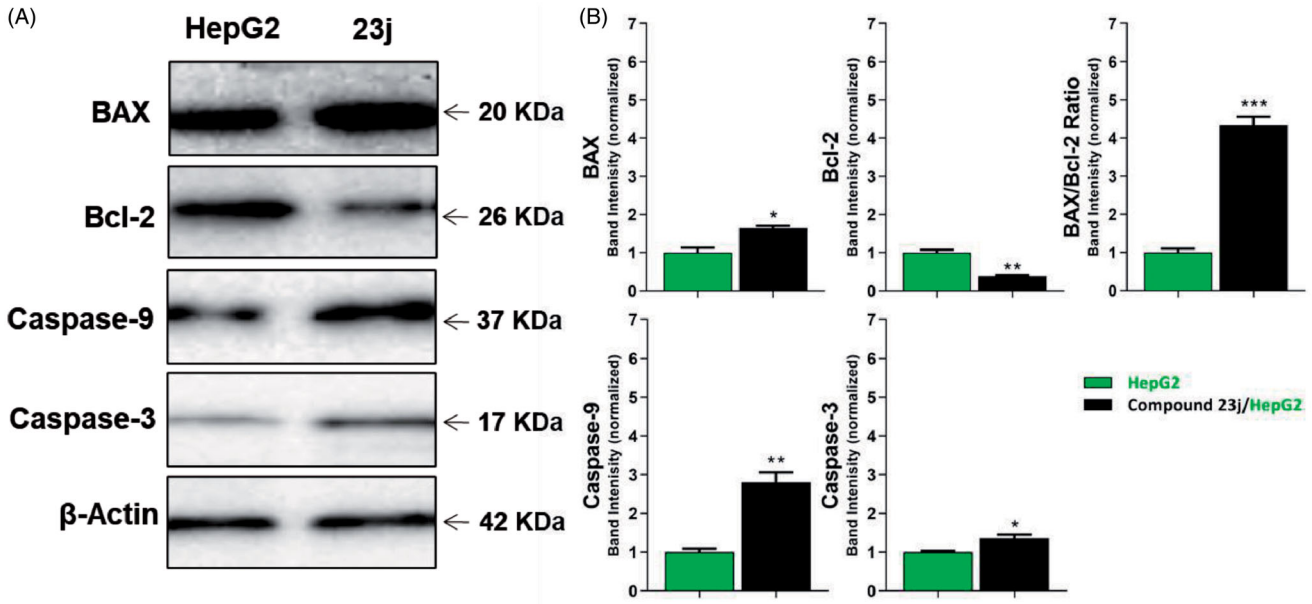

Figure 8. The immunoblotting of BAX, Bcl-2, Caspase-9, and Caspase-3 (Normalized to β-actin). $^{*}p < .05$, $^{**}p < .01$, $^{***}p < .001$.

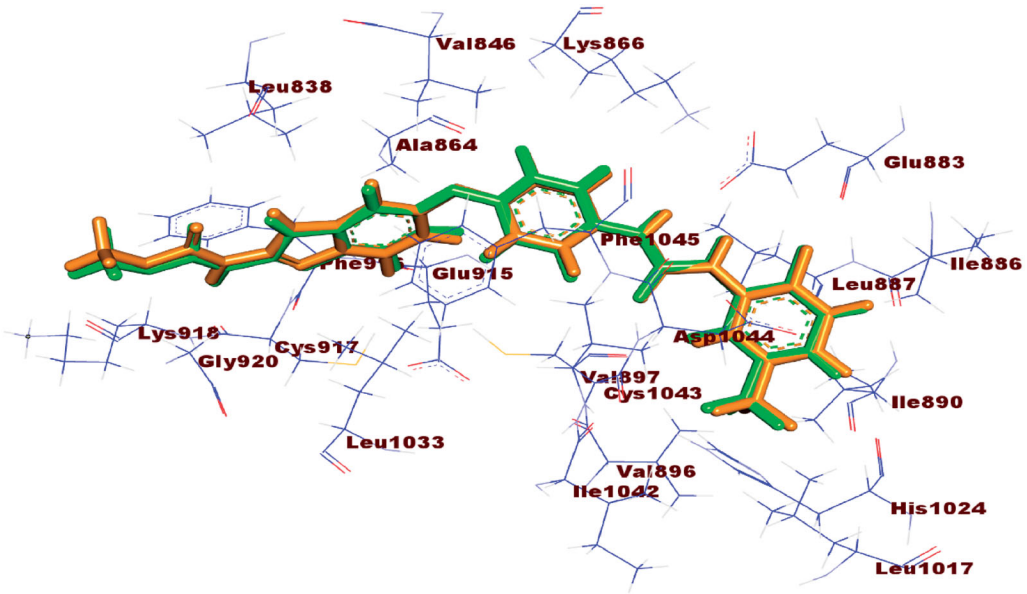

Figure 9. Alignment of the co-crystallised pose (green) and the redocked pose (Orange) of the same ligand inside the protein.

Table 5. The calculated ΔG of the synthesised candidates and sorafenib (ΔG in kcal/mole).

Comp. No.	ΔG [kcal mol^{-1}]	Compound	ΔG [kcal mol^{-1}]
23a	−22.15	**23j**	−23.87
23b	−22.86	**23k**	−22.98
23c	−23.25	**23l**	−23.26
23d	−21.65	**23m**	−22.88
23e	−22.97	**23n**	−22.98
23f	−21.47	**24a**	−21.30
23g	−23.00	**24b**	−21.71
23h	−22.37	**24c**	−22.76
23i	−23.63	**Sorafenib**	−22.48

4.1.1. General procedure for synthesis of compounds 18a–n

A mixture of **17** (2 mmol) and appropriate amines namely, ethylamine, *n*-butylamine, *sec*-butylamine, *tert*-butylamine, cyclopentylamine, cyclohexylamine, 4-aminoacetophenone, 3-chloroaniline, 4-chloroaniline, 2,5-dichloroaniline, 4-flouroaniline, 2-hydroxyaniline, 4-hydroxyaniline, and 2-hydroxy-4-nitroaniline (2 mmol) was stirred in acetonitrile (50 ml) in the presence of trimethylamine (1 ml) for 8 h. The obtained precipitates were filtered and crystallised from ethanol to give the corresponding derivatives, **18a–n**, respectively.

4.1.1.1. 4-(2-Chloroacetamido)-N-ethylbenzamide (18a). Yellow crystal (yield, 80%); m.p. = 190 − 192 °C; FT-IR (ν_{max}, cm^{-1}): 3376, 3273 (NH), 2971(C–H aliphatic), 1709, 1636 (C=O), 1605 (C=N); ^{1}H NMR (400 MHz, DMSO-d$_6$) δ 10.49 (s, 1H), 8.36 (s, 1H), 7.80 (d, J = 9.7 Hz, 2H), 7.63 (d, J = 8.3 Hz, 2H), 4.26 (s, 2H), 3.29 − 3.21 (q, 2H), 1.14 − 1.05 (t, 3H).; ^{13}C NMR (101 MHz, DMSO-d$_6$) δ 165.73 (2C), 165.40 (2C), 141.29, 130.24, 128.37, 44.04, 34.42, 15.43, 15.20; Anal. Calcd. for $C_{11}H_{13}ClN_2O_2$ (240.68): C, 54.89; H, 5.44; N, 11.64. Found: C, 54.72; H, 5.20; N, 11.46%.

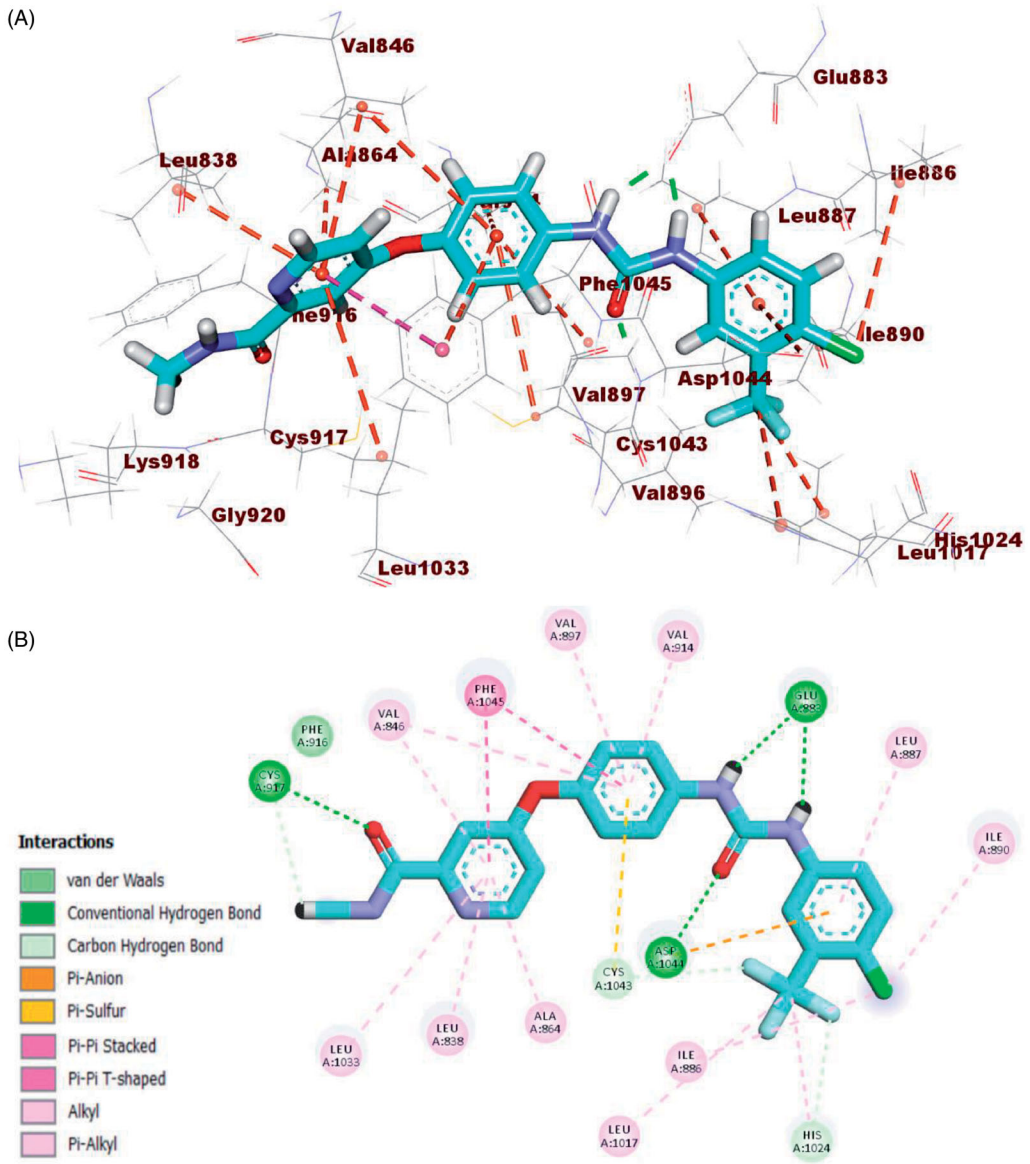

Figure 10. (A) 3D binding mode of sorafenib into VEGFR-2. (B) 2D binding mode sorafenib into VEGFR-2.

4.1.1.2. **N-*Butyl-4–(2-chloroacetamido)benzamide (18b).*** White crystal (yield, 85%); m.p. = 170 – 172 °C; FT-IR (ν_{max}, cm^{-1}): 3369, 3263 (NH), 3185 (NH), 3099 (C–H aromatic), 2960 (C–H aliphatic), 1706, 1633 (C=O), 1606 (C=N); ^{1}H NMR (400 MHz, DMSO-d_6) δ 10.57 (s, 1H), 8.33 (s, 1H), 7.80 (dd, J = 8.8, 1.8 Hz, 2H), 7.66 – 7.61 (m, 2H), 4.27 (s, 2H), 3.25 – 3.18 (m, 2H), 1.51 – 1.43 (m, 2H), 1.33 – 1.26 (m, 2H), 0.89 – 0.84 (m, 3H); ^{13}C NMR (101 MHz, DMSO-d_6) δ 165.93, 165.41, 141.30, 130.27, 128.67, 128.31, 119.43, 118.44, 44.44, 44.01, 31.74, 20.12, 14.18; MS (*m/z*): 269 (M^+ + 1, 100%). Anal. Calcd. for $C_{13}H_{17}ClN_2O_2$ (268.74): C, 58.10; H, 6.38; N, 10.42. Found: C, 58.38; H, 6.61; N, 10.32%.

4.1.1.3. **N-*(Sec-butyl)-4-(2-chloroacetamido)benzamide (18c).*** White crystals (yield 78%); m.p. = 180–182 °C; IR (KBr) ν cm^{-1}: 3307, 3113 (NH), 2969, 2933 (CH aliphatic), 1684, 1625 (C=O); ^{1}H NMR (400 MHz, DMSO-d_6) δ 10.54 (s, 1H), 8.06 (d, J = 6.1 Hz, 1H), 7.82 (d, J = 6.3 Hz, 2H), 7.65 (d, J = 7.9 Hz, 2H), 4.28 (s, 2H), 3.89 (dq, J = 11.8, 6.8 Hz, 1H), 1.56 – 1.41 (m, 2H), 1.11 (d, J = 5.1 Hz, 3H), 0.84 (d, J = 4.7 Hz, 3H); ^{13}C NMR (101 MHz, DMSO-d_6) δ 165.46, 165.38, 141.25, 130.45, 128.64, 119.33, 118.74, 118.44, 46.76, 44.05, 29.31, 20.69, 11.29; Anal. Calcd. for $C_{13}H_{17}ClN_2O_2$ (268.74): C, 58.10; H, 6.38; N, 10.42. Found: C, 58.06; H, 6.65; N, 10.29%.

4.1.1.4. **N-*(Tert-butyl)-4-(2-chloroacetamido)benzamide (18d).*** Yellow crystals (yield 68%); m.p. = 190–192 °C; IR (KBr) ν cm^{-1}: 3314 (NH), 2975 (CH aliphatic), 1666, 1628 (C=O), 1606 (C=N); Anal. Calcd. for $C_{13}H_{17}ClN_2O_2$ (268.74): C, 58.10; H, 6.38; N, 10.42. Found: C, 58.31; H, 6.55; N, 10.59%.

4.1.1.5. ***4-(2-Chloroacetamido)-N-cyclopentylbenzamide (18e).*** White crystals (yield 82%); m.p. = 230–232 °C; IR (KBr) ν cm^{-1}: 3290 (NH), 2961 (CH aliphatic), 1680, 1624 (C=O); ^{1}H NMR (400 MHz, DMSO-d_6) δ 10.77 (s, 1H), 8.20 (d, J = 7.3 Hz, 1H), 7.81 (d, J = 8.7 Hz, 2H), 7.66 (d, J = 8.7 Hz, 2H), 4.31 (s, 2H), 3.03 (qd, J = 7.2, 4.2 Hz, 1H), 1.87 – 1.82 (m, 2H), 1.66 (tt, J = 4.5, 2.5 Hz, 2H), 1.50 (qd, J = 7.7, 6.9, 3.9 Hz, 4H); ^{13}C NMR (101 MHz, DMSO-d_6) δ 165.75, 165.42, 141.35, 130.26, 128.76, 119.28, 118.81, 118.36, 51.46, 44.00, 32.54, 31.05, 24.05, 8.93; MS (*m/z*): 281 (M^+ + 1, 100%); Anal. Calcd. for $C_{14}H_{17}ClN_2O_2$ (280.75): C, 59.89; H, 6.10; N, 9.98. Found: C, 59.50; H, 6.04; N, 10.25%.

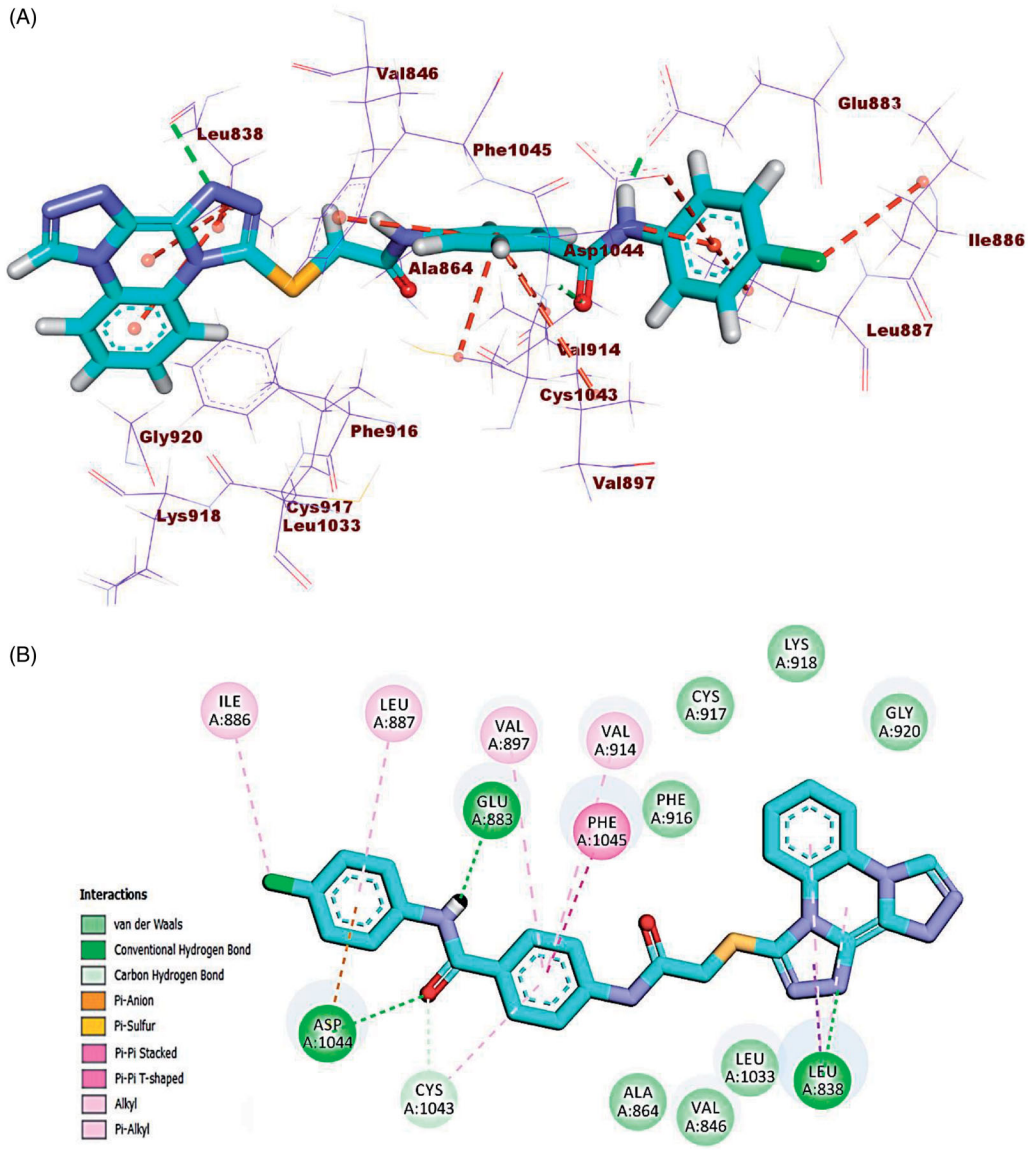

Figure 11. (A) 3D binding mode of compound **23i** into VEGFR-2. (B) 2D binding mode of compound **23i** into VEGFR-2.

4.1.1.6. 4-(2-Chloroacetamido)-N-cyclohexylbenzamide (18f). White crystals (yield 78%); m.p. = 220–222 °C; FT-IR ((ν_{max}, cm^{-1}): 3286 (NH), 3042 (C–H aromatic), 2938, 2854 (C–H aliphatic), 1681, 1624 (C=O), 1610 (C=N); ^{1}H NMR (400 MHz, DMSO-d_6) δ 10.52 (s, 1H), 8.08 (d, J = 7.9 Hz, 1H), 7.83 – 7.77 (m, 2H), 7.65 – 7.59 (m, 2H), 4.26 (s, 2H), 3.72 (s, 1H), 1.78 (d, J = 7.1 Hz, 2H), 1.71 (d, J = 8.4 Hz, 2H), 1.58 (d, J = 12.8 Hz, 1H), 1.27 (dd, J = 11.4, 8.6 Hz, 4H), 1.12 (q, J = 10.8, 9.3 Hz, 1H); ^{13}C NMR (101 MHz, DMSO-d_6) δ 165.38, 165.15, 141.24, 130.41, 129.07, 128.80, 128.47, 119.35, 118.86, 118.41, 48.79, 48.66, 44.42, 44.02, 25.63; Anal. Calcd. for $C_{15}H_{19}ClN_2O_2$ (294.77): C, 61.12; H, 6.50; N, 9.50. Found: C, 60.88; H, 6.39; N, 9.25%.

4.1.1.7. N-(4-Acetylphenyl)-4-(2-chloroacetamido)benzamide (18g). White crystals (yield 80%); m.p. = 250–252 °C; FT-IR (ν_{max}, cm^{-1}): 3326 (NH), 3062 (C–H aromatic), 1674, 1655 (C=O), 1596 (C=N); ^{1}H NMR (400 MHz, DMSO-d_6) δ 10.61 (s, 1H), 10.46 (s, 1H), 7.98 – 7.90 (m, 6H), 7.72 (s, 2H), 4.29 (s, 2H), 2.53 (s, 3H); ^{13}C NMR (101 MHz, DMSO-d_6) δ 197.08, 165.69(2 C), 165.57(2 C), 144.14, 142.15, 132.33, 129.90, 129.85, 129.60, 129.26, 119.97, 119.66, 118.65, 44.05, 27.16; Anal. Calcd. for $C_{17}H_{15}ClN_2O_3$ (330.76): C, 61.73; H, 4.57; N, 8.47. Found: C, 61.44; H, 4.39; N, 8.29%.

4.1.1.8. 4-(2-Chloroacetamido)-N-(3-chlorophenyl)benzamide (18h). Yellow crystal (yield, 75%); m.p. = 190 – 192 °C; FT-IR (v max, cm^{-1}): 3291 (NH), 1676, 1644 (C=O), 1593 (C=N); ^{1}H NMR (400 MHz, DMSO-d_6) δ 10.60 (s, 1H), 10.30 (s, 1H), 7.95 – 7.94 (m, 2H), 7.93 (d, J = 1.9 Hz, 1H), 7.74 – 7.68 (m, 3H), 7.36 (t, J = 8.1 Hz, 1H), 7.14 – 7.12 (m, 1H), 4.29 (s, 2H); ^{13}C NMR (101 MHz, DMSO-d_6) δ 165.56, 165.53, 142.07, 141.20, 141.14, 133.33, 129.86, 129.41, 129.12, 120.24, 119.93, 119.03, 118.66, 118.59, 44.05; Anal. Calcd. for $C_{15}H_{12}Cl_2N_2O_2$ (323.17): C, 55.75; H, 3.74; N, 8.67. Found: C, 55.64; H, 3.63; N, 8.45%.

4.1.1.9. 4-(2-Chloroacetamido)-N-(4-chlorophenyl)benzamide (18i). Yellow crystal (yield, 83%); m.p. = 228 – 230 °C; FT-IR (ν_{max}, cm^{-1}): 3324 (NH), 1666 (C=O amide), 1595 (C=N); ^{1}H NMR (400 MHz, DMSO-d_6) δ 10.59 (s, 1H), 10.27 (s, 1H), 7.93 (d, J = 8.6 Hz, 2H), 7.79 (d, J = 8.9 Hz, 2H), 7.72 (d, J = 8.7 Hz, 2H), 7.38 (d, J = 8.8 Hz, 2H), 4.29 (s, 2H); ^{13}C NMR (101 MHz, DMSO-d_6) δ 165.53 (2C), 165.36

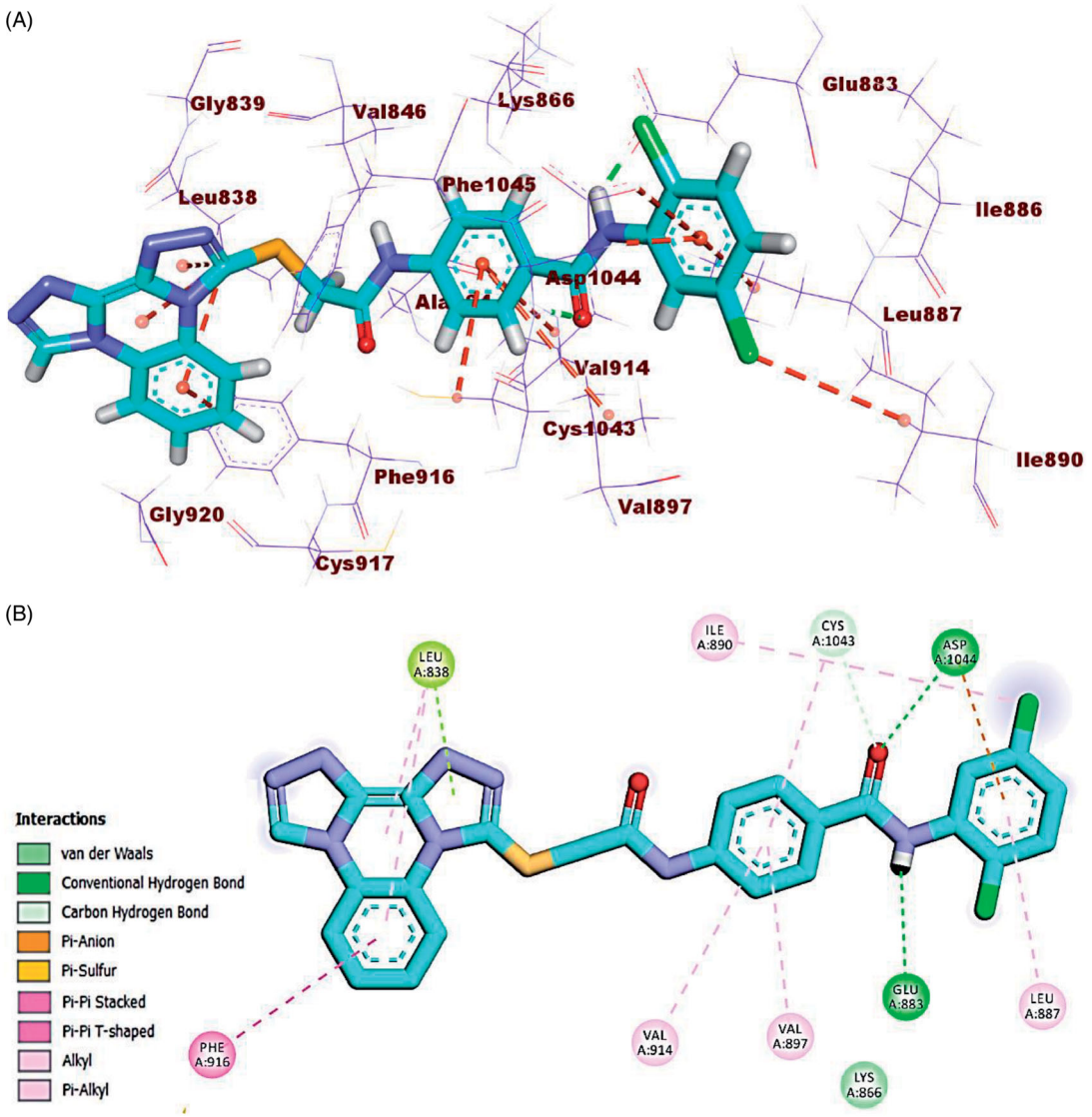

Figure 12. (A) 3D binding mode of compound **23j** into VEGFR-2. (B) 2D binding mode of compound **23j** into VEGFR-2.

(2C), 141.98, 138.67, 130.01, 129.36 (2C), 129.08, 128.58, 128.30, 127.56, 118.63, 44.05; Anal. Calcd. for $C_{15}H_{12}Cl_2N_2O_2$ (322.17): C, 55.75; H, 3.74; N, 8.67. Found: C, 55.59; H, 3.57; N, 8.40%.

4.1.1.10. 4-(2-Chloroacetamido)-N-(2,5-dichlorophenyl)benzamide (18j).

Yellow crystal (yield, 77%); m.p. = 195 – 197 °C; FT-IR (ν_{max}, cm^{-1}): 3277, 3104 (NH), 3033 (C–H aromatic), 1770, 1679 (C=O), 1606 (C=N); ^{1}H NMR (400 MHz, DMSO-d_6) δ 10.63 (s, 1H), 10.03 (s, 1H), 7.96 (d, J = 8.7 Hz, 2H), 7.73 (dd, J = 5.6, 3.0 Hz, 3H), 7.57 (d, J = 8.6 Hz, 1H), 7.34 (dd, J = 8.6, 2.5 Hz, 1H), 4.29 (s, 2H); ^{13}C NMR (101 MHz, DMSO-d_6) δ 165.60 (2 C), 165.26, 142.26, 136.86, 131.87, 131.81, 130.80, 129.48 (2C), 129.19, 128.97 (2C), 118.75, 44.02; Anal. Calcd. for $C_{15}H_{11}Cl_3N_2O_2$ (357.61): C, 50.38; H, 3.10; N, 7.83. Found: C, 50.42; H, 3.18; N, 7.64%.

4.1.1.11. 4-(2-Chloroacetamido)-N-(4-fluorophenyl)benzamide (18k).

White crystal (yield, 70%); m.p. = 238–240 °C; FT-IR (ν_{max}, cm^{-1}); 3325 (NH), 1666, 1643 (C=O), 1611 (C=N); ^{1}H NMR (400 MHz, DMSO-d_6) δ 10.66 (s, 1H), 10.23 (s, 1H), 7.95 (d, J = 7.0 Hz, 2H), 7.82 – 7.70 (m, 4H), 7.17 (s, 2H), 4.31 (t, J = 2.8 Hz, 2H); ^{13}C NMR (101 MHz, DMSO-d_6) δ 165.54, 165.21, 141.91, 136.06, 136.02, 130.12, 129.28, 129.04, 122.15, 119.45, 119.02, 118.63, 116.11, 115.88, 44.06; Anal. Calcd. for $C_{15}H_{12}ClFN_2O_2$ (306.72): C, 58.74; H, 3.94; N, 9.13. Found: C, 58.55; H, 3.89; N, 9.05%.

4.1.1.12. 4-(2-Chloroacetamido)-N-(2-hydroxyphenyl)benzamide (18l).

Brown crystal (yield, 65%); m.p. = 192 – 194 °C; FT-IR (ν_{max}, cm^{-1}): 3262, 3190 (NH), 3064 (C–H aromatic), 2952 (C–H aliphatic), 1735, 1683 (C=O), 1600 (C=N); ^{1}H NMR (400 MHz, DMSO-d_6) δ 10.70 (s, 1H), 10.00 (s, 1H), 9.49 (s, 1H), 8.11–8.02 (m, 2H), 8.02–7.91 (m, 2H), 7.12 – 6.73 (m, 4H), 4.32 (s, 2H); ^{13}C NMR (101 MHz, DMSO-d_6) δ 165.77, 165.24, 165.07, 163.82 (2C), 149.77, 144.89, 143.80, 141.98, 131.61, 129.69 (2C), 126.39, 124.39, 44.07; Anal. Calcd. for $C_{15}H_{13}ClN_2O_3$ (304.72): C, 59.12; H, 4.30; N, 9.19. Found: C, 59.01; H, 4.14; N, 8.92%.

4.1.1.13. 4-(2-Chloroacetamido)-N-(4-hydroxyphenyl)benzamide (18m).

Brown crystal (yield, 85%); m.p. >300 °C; FT-IR (ν_{max}, cm^{-1}): 3309, 3104 (NH), 3033 (C–H aromatic), 1770, 1671 (C=O), 1607 (C=N); ^{1}H NMR (400 MHz, DMSO-d_6) δ 10.81 (s, 1H), 10.29 (s, 1H), 9.95 (s, 1H), 8.11 (d, J = 9.2 Hz, 2H), 7.85 – 7.80 (m, 2H), 7.50 (d,

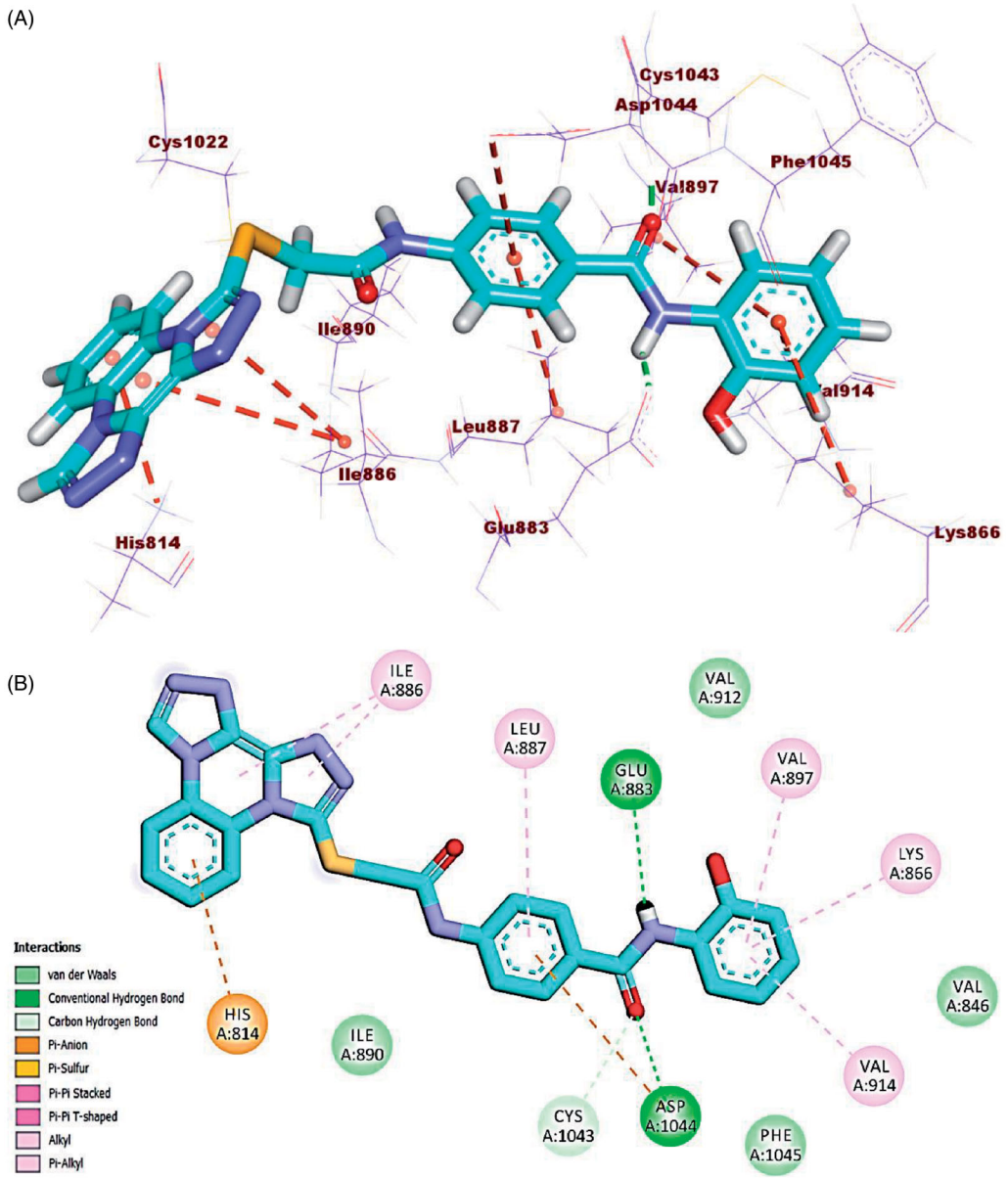

Figure 13. (A) 3D binding mode of compound **23l** into VEGFR-2. (B) 2D binding mode of compound **23l** into VEGFR-2.

$J = 8.4$ Hz, 2H), 6.72 (d, $J = 8.3$ Hz, 2H), 4.30 (d, $J = 4.1$ Hz, 2H); Anal. Calcd. for $C_{15}H_{13}ClN_2O_3$ (304.73): C, 59.12; H, 4.30; N, 9.19. Found: C, 59.32; H, 4.15; N, 8.95%.

4.1.1.14. 4-(2-Chloroacetamido)-N-(2-hydroxy-4-nitrophenyl)benzamide (18n).

Greenish yellow crystal (yield, 60%); m.p. = 198–200 °C; FT-IR (ν_{max}, cm^{-1}): 3596, 3409 (NH), 3074 (C–H aromatic), 1700, 1652 (C=O), 1602 (C=N); ^{1}H NMR (400 MHz, DMSO-d_6) δ 11.15 (s, 1H), 10.66 (s, 1H), 9.51 (s, 1H), 8.22 (d, $J = 8.3$ Hz, 1H), 7.96 (d, $J = 8.3$ Hz, 2H), 7.85 – 7.67 (m, 4H), 4.30 (s, 2H); ^{13}C NMR (101 MHz, DMSO-d_6) δ 165.61, 165.05 (2C), 148.61 (2C), 143.65, 142.42, 133.57, 129.12 (2 C), 122.04, 118.83, 115.16, 109.46, 44.07; Anal. Calcd. for $C_{15}H_{12}ClN_3O_5$ (349.72): C, 51.52; H, 3.46; N, 12.02. Found: C, 51.33; H, 3.57; N, 11.87%.

4.1.2. General procedure for the synthesis of compounds 22a–c

A mixture of **17** (2 mmol) and the acid hydrazides **21a–c** namely, 2-chlorobenzohydrazide, 3-chlorobenzohydrazide, and 2-hydroxybenzohyazide (2 mmol) was allowed to stir in acetonitrile (50 ml) in the presence of trimethylamine (1 ml) for 8 h. The precipitated products were filtered, dried, and crystalised from ethanol to give the diamide intermediated, **22a–c**, respectively.

4.1.2.1. 2-Chloro-N-(4-(2-(2-chlorobenzoyl)hydrazine-1-carbonyl)-phenyl)acetamide (22a).

White crystal (yield, 85%); m.p. = 230 – 232 °C; FT-IR (ν_{max}, cm^{-1}): 3409, 3249 (NH), 3074 (C–H aromatic), 1673, 1650 (C=O), 1603 (C=N); ^{1}H NMR (400 MHz, DMSO-d_6) δ 10.65 (s, 1H), 10.55 (s, 1H), 10.38 (s, 1H), 7.92 (d, $J = 7.5$ Hz, 2H), 7.72 (d, $J = 7.6$ Hz, 2H), 7.56 – 7.46 (m, 4H), 4.33 – 4.28 (m, 2H); Anal. Calcd. for $C_{16}H_{13}Cl_2N_3O_3$ (366.19): C, 52.48; H, 3.58; N, 11.47. Found: C, 52.72; H, 3.48; N, 11.34%.

4.1.2.2. 2-Chloro-N-(4-(2-(3-chlorobenzoyl)hydrazine-1-carbonyl)-phenyl)acetamide (22b).

Yellow crystal (yield, 80%); m.p. = 235 – 237 °C; FT-IR (ν_{max}, cm^{-1}): 3409, 3283 (NH), 3074 (C–H aromatic), 1676, 1645 (C=O), 1604 (C=N); ^{1}H NMR (400 MHz, DMSO-

Table 6. ADME screening of the designed compounds

Comp.	BBB level[a]	Solubility level[b]	Absorption level[c]	CYP2D6 prediction[d]	PPB prediction[e]
23a	4	2	0	FALSE	FALSE
23b	4	2	1	FALSE	FALSE
23c	4	2	1	FALSE	FALSE
23d	4	2	1	FALSE	FALSE
23e	4	2	1	FALSE	FALSE
23f	4	1	2	FALSE	FALSE
23g	4	2	2	FALSE	FALSE
23h	4	1	2	FALSE	FALSE
23ai	4	1	2	FALSE	FALSE
23j	4	1	2	FALSE	FALSE
23k	4	1	1	FALSE	FALSE
23l	4	2	2	FALSE	FALSE
23m	4	2	2	FALSE	FALSE
23n	4	2	3	FALSE	FALSE
24a	4	1	2	FALSE	FALSE
24b	4	1	2	FALSE	FALSE
24c	4	2	3	FALSE	FALSE
Sorafenib	4	1	0	FALSE	TRUE

[a]BBB: very high (0), high (1), medium (2), low (3), or very low (4).
[b]Solubility level: very low (1), low (2), good (3), or optimal (4).
[c]Absorption level: good (0), moderate (1), poor (2), or very poor (3).
[d]CYP2D6: inhibitor (TRUE) or non-inhibitor (FALSE).
[e]PPB: less than 90% (FALSE) or more than 90% (TRUE).

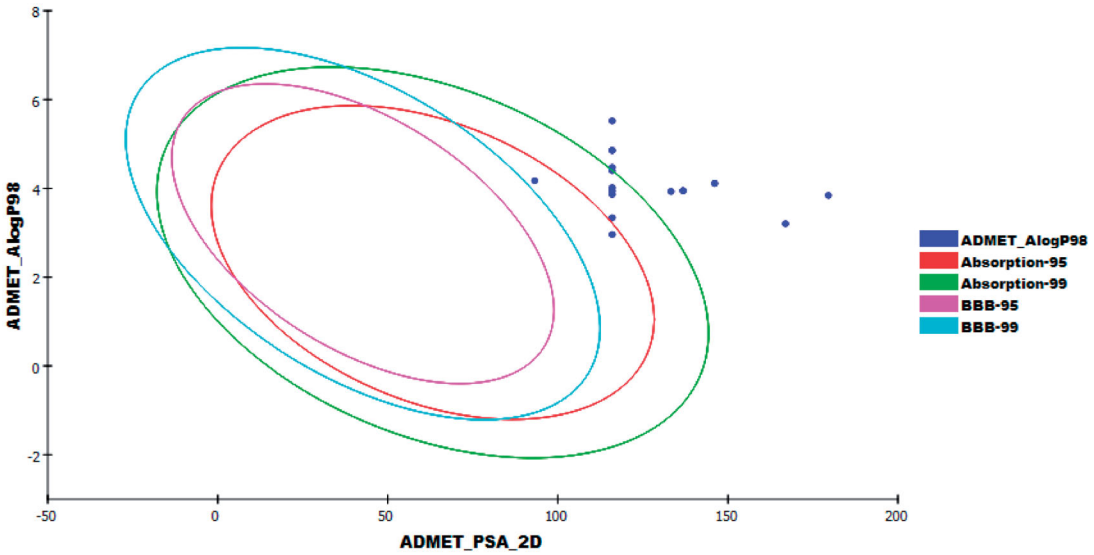

Figure 14. The ADME plot of the synthesised compounds.

d_6) δ 10.63 (s, 2H), 10.51 (s, 1H), 7.91 (dd, $J = 19.0$, 9.7 Hz, 4H), 7.74 – 7.66 (m, 3H), 7.58 (d, $J = 6.4$ Hz, 1H), 4.30 (t, $J = 2.4$ Hz, 2H); ^{13}C NMR (101 MHz, DMSO-d_6) δ 165.67, 165.58 (2C), 165.00, 142.13, 134.92, 133.83, 129.11, 128.88, 127.83 (2C), 127.59, 119.58, 119.13, 118.75, 44.06; Anal. Calcd. for $C_{16}H_{13}Cl_2N_3O_3$ (366.19): C, 52.48; H, 3.58; N, 11.47. Found: C, 52.71; H, 3.62; N, 11.60%.

4.1.2.3. 2-Chloro-N-(4–(2-(2-hydroxybenzoyl)hydrazine-1-carbonyl)-phenyl)acetamide (22c).

Yellow crystal (yield, 80%); m.p. = 233 – 235 °C; FT-IR (ν_{max}, cm^{-1}): 3272 (NH), 1687, 1661 (C=O), 1600 (C=N); ^{1}H NMR (400 MHz, DMSO-d_6) δ 11.97 (s, 1H), 10.69 (d, $J = 9.7$ Hz, 2H), 10.63 (s, 1H), 7.93 (d, $J = 8.0$ Hz, 3H), 7.75 (d, $J = 8.1$ Hz, 2H), 7.44 (d, $J = 8.6$ Hz, 1H), 6.96 (q, $J = 8.4$, 7.4 Hz, 2H), 4.32 (s, 2H); ^{13}C NMR (101 MHz, DMSO-d_6) δ 168.25, 165.62, 165.47, 159.76, 159.72, 142.21, 129.14, 128.87, 128.65, 127.68, 119.58, 119.16, 118.79, 118.12, 114.98, 44.07; Anal. Calcd. for $C_{16}H_{14}ClN_3O_4$ (347.76): C, 55.26; H, 4.06; N, 12.08. Found: C, 55.45; H, 3.83; N, 11.90%.

4.1.3. General procedure for the synthesis of compounds 23a–n

A mixture of potassium salt of bis([1, 2, 4]triazolo)[4,3-*a*:3′,4′-*c*]quinoxaline-3-thiol **14** (0.5 g, 0.001 mol) and 4-(2-chloroacetamido)-*N*-(substituted)benzamide **18a**–**n** (0.001 mol) in DMF (50 ml) was heated on a water bath for 6 h. After cooling to room temperature, the reaction mixture was poured on crushed ice. The obtained precipitates were collected by filtration, dried, and crystalised from ethanol to give the target compounds **23a**–**n**.

4.1.3.1. 4-(2-(Bis([1, 2, 4]triazolo)[4,3-a:3′,4′-c]quinoxalin-3-ylthio)acetamido)-N-ethylbenzamide (23a).

White crystal (yield, 70%); m.p. = 260–262 °C. FT-IR (ν_{max}, cm^{-1}): 3267 (NH), 1700, 1655 (C=O), 1596 (C=N); ^{1}H NMR (700 MHz, DMSO-d_6) δ 10.69 (s, 1H), 10.12 (s, 1H), 8.35 (dq, $J = 11.5$, 3.7, 3.1 Hz, 2H), 7.86 (dd, $J = 8.1$, 3.1 Hz, 1H), 7.85 – 7.80 (m, 2H), 7.75 – 7.69 (m, 2H), 7.69 – 7.65 (m, 1H), 7.63 (dt, $J = 10.1$, 5.1 Hz, 1H), 4.41 (d, $J = 3.4$ Hz, 2H), 3.32 – 3.25 (m, 2H), 1.16 – 1.09 (m, 3H); ^{13}C NMR (176 MHz, DMSO-d_6) δ 166.67, 165.83, 151.65, 141.85 (2C), 138.29, 135.59,

Table 7. Toxicity study of the synthesised compounds.

Comp.	FDA rodent carcinogenicity (mouse- female)	Carcinogenic potency TD_{50} (rat)[a]	Rat maximum tolerated dose (feed)[b]	Developmental toxicity potential	Rat oral LD_{50}[b]	Rat chronic LOAEL[b]
23a	Non-carcinogen	35.802	0.099	Non-toxic	2.209	0.153
23b	Non-carcinogen	33.907	0.145	Non-toxic	1.900	0.329
23c	Non-carcinogen	0.543	0.114	Non-toxic	1.899	0.206
23d	Non-carcinogen	10.185	0.075	Non-toxic	1.978	0.084
23e	Non-carcinogen	0.857	0.088	Non-toxic	0.729	0.221
23f	Non-carcinogen	0.794	0.083	Non-toxic	0.619	0.192
23g	Non-carcinogen	7.641	0.087	Non-toxic	1.071	0.094
23h	Non-carcinogen	4.519	0.133	Non-toxic	0.720	0.072
23i	Non-carcinogen	4.519	0.133	Non-toxic	1.140	0.067
23j	Non-carcinogen	4.056	0.105	Non-toxic	0.546	0.064
23k	Non-carcinogen	4.882	0.144	Non-toxic	0.592	0.073
23l	Non-carcinogen	37.552	0.362	Non-toxic	0.663	0.134
23m	Non-carcinogen	37.552	0.362	Non-toxic	0.864	0.115
23n	Non-carcinogen	13.503	0.262	Non-toxic	0.769	0.094
24a	Non-carcinogen	5.280	0.143	Non-toxic	2.477	0.155
24b	Non-carcinogen	5.080	0.143	Non-toxic	1.754	0.089
24c	Non-carcinogen	44.001	0.391	Non-toxic	1.350	0.211
Sorafenib	Single-carcinogen	14.244	0.089	Toxic	0.823	0.005

[a]Unit: mg/kg body weight/day.
[b]Unit: g/kg body weight.

129.91, 128.73, 128.52 (2C), 128.34, 128.32 (2C), 124.07, 118.76 (2C), 117.13, 34.45 (2C), 15.33; Anal. Calcd. for $C_{21}H_{18}N_8O_2S$ (446.49): C, 56.49; H, 4.06; N, 25.10. Found: C, 56.21; H, 4.15; N, 24.95%.

4.1.3.2. 4-(2-(Bis([1, 2, 4]triazolo)[4,3-a:3′,4′-c]quinoxalin-3-ylthio)acetamido)-N-butylbenzamide (23b). Yellowish white crystal (yield, 70%); m.p. = 252–254 °C. FT-IR (ν_{max}, cm^{-1}): 3299 (NH), 2928 (CH aliphatic), 1676, 1631 (C=O); ^{1}H NMR (700 MHz, DMSO-d_6) δ 10.68 (s, 1H), 10.02 (s, 1H), 8.65 – 8.58 (m, 1H), 8.50 – 8.45 (m, 1H), 8.33 (q, J = 4.9 Hz, 1H), 7.86 – 7.79 (m, 2H), 7.75 (p, J = 7.6, 7.2 Hz, 2H), 7.65 (d, J = 8.4 Hz, 2H), 4.57 (s, 2H), 3.25 (p, J = 6.6, 5.4 Hz, 2H), 1.50 (q, J = 7.5 Hz, 2H), 1.33 (q, J = 8.0 Hz, 2H), 0.94 – 0.88 (m, 3H); ^{13}C NMR (176 MHz, DMSO-d_6) δ 165.93, 165.90, 147.72, 142.11, 141.56, 139.35, 138.78, 130.08, 128.54, 128.37, 128.35, 124.09, 123.20, 118.76, 118.58, 118.07, 39.29, 38.88, 31.78, 20.15, 14.22; MS (*m/z*): 475 (M^+ + 1, 50%); Anal. Calcd. for $C_{23}H_{22}N_8O_2S$ (474.54): C, 58.21; H, 4.67; N, 23.61. Found: C, 58.05; H, 4.60; N, 23.55%.

4.1.3.3. 4-(2-(Bis([1, 2, 4]triazolo)[4,3-a:3′,4′-c]quinoxalin-3-ylthio)acetamido)-N-(sec-butyl)benzamide (23c). White crystal (yield, 72%); m.p. = 245–247 °C. FT-IR (ν_{max}, cm^{-1}): 3266, 3127 (NH), 2965, 2910 (CH aliphatic), 1701, 1636 (C=O), 1605 (C=N); ^{1}H NMR (700 MHz, DMSO-d_6) δ 10.68 (s, 1H), 10.01 (s, 1H), 8.58 (d, J = 8.1 Hz, 1H), 8.45 (d, J = 7.9 Hz, 1H), 8.04 (d, J = 8.4 Hz, 1H), 7.83 (d, J = 8.3 Hz, 2H), 7.73 (p, J = 7.6 Hz, 2H), 7.65 (d, J = 8.3 Hz, 2H), 4.57 (s, 2H), 3.90 (dd, J = 14.5, 7.5 Hz, 1H), 1.51 (ddq, J = 29.9, 15.4, 8.3, 7.7 Hz, 2H), 1.13 (d, J = 6.6 Hz, 3H), 0.87 (d, J = 7.5 Hz, 3H); ^{13}C NMR (176 MHz, DMSO-d_6) δ 165.88, 165.48, 147.74, 142.07, 141.52, 139.32, 138.77, 130.27, 128.63 (2C), 128.34, 128.32, 124.04, 123.15, 118.69 (2C), 118.56, 118.03, 46.82, 38.89, 29.34, 20.77, 11.25; MS (*m/z*): 475 (M^+ + 1, 60%); Anal. Calcd. for $C_{23}H_{22}ClN_8O_2S$ (474.54): C, 58.21; H, 4.67; N, 23.61. Found: C, 57.98; H, 4.62; N, 23.57%.

4.1.3.4. 4-(2-(Bis([1, 2, 4]triazolo)[4,3-a:3′,4′-c]quinoxalin-3-ylthio)acetamido)-N-(tert-butyl)benzamide (23d). Faint yellow crystal (yield, 75%); m.p. = 248–250 °C. FT-IR (ν_{max}, cm^{-1}): 3439, 3104 (NH), 3051 (CH aromatic), 2968, 2929 (CH aliphatic), 1651 (C=O), 1600 (C=N); ^{1}H NMR (700 MHz, DMSO-d_6) δ 10.67 (s, 1H), 10.03 (s, 1H), 8.61 (d, J = 8.0 Hz, 1H), 8.50 – 8.47 (m, 1H), 7.79 (t, J = 6.9 Hz, 3H), 7.76 (d, J = 8.1 Hz, 2H), 7.63 (d, J = 8.1 Hz, 2H), 4.57 (s, 2H), 1.38 (s, 9H); ^{13}C NMR (176 MHz, DMSO-d_6) δ 166.06, 165.85, 147.74, 142.13, 141.39, 139.37, 138.78, 131.16, 128.74 (2C), 128.38, 128.37, 124.12, 123.23, 118.60, 118.57 (2C), 118.08, 51.16, 38.87, 29.11 (3C); MS (*m/z*): 475 (M^+ + 1, 100%); Anal. Calcd. for $C_{23}H_{22}N_8O_2S$ (474.54): C, 58.21; H, 4.67; N, 23.61. Found: C, 58.05; H, 4.55; N, 23.44%.

4.1.3.5. 4-(2-(Bis([1, 2, 4]triazolo)[4,3-a:3′,4′-c]quinoxalin-3-ylthio)acetamido)-N-cyclopentylbenzamide (23e). Yellow crystal (yield, 77%); m.p. = 244–246 °C. FT-IR (ν_{max}, cm^{-1}): 3262, 3124 (NH), 2950, 2905 (CH aliphatic), 1699, 1636 (C=O), 1607 (C=N); ^{1}H NMR (700 MHz, DMSO-d_6) δ 10.68 (s, 1H), 10.02 (s, 1H), 8.61 (dd, J = 8.0, 1.6 Hz, 1H), 8.47 (dd, J = 7.8, 1.8 Hz, 1H), 8.17 (d, J = 7.3 Hz, 1H), 7.83 (d, J = 8.6 Hz, 2H), 7.76 (ddd, J = 8.9, 7.6, 1.6 Hz, 2H), 7.65 (d, J = 8.6 Hz, 2H), 4.57 (s, 2H), 4.21 (q, J = 7.1 Hz, 1H), 1.88 (dtd, J = 12.0, 8.8, 7.9, 4.4 Hz, 2H), 1.70 (dt, J = 9.6, 5.3 Hz, 2H), 1.56 – 1.51 (m, 4H); ^{13}C NMR (176 MHz, DMSO-d_6) δ 165.88, 165.73, 147.73, 142.12, 141.53, 139.36, 138.78, 130.15, 128.70 (2C), 128.37, 128.35, 124.10, 123.21, 118.66 (2C), 118.59, 118.06, 51.34, 38.87, 32.61 (2C), 24.09 (2C); MS (*m/z*): 487 (M^+ + 1, 65%); Anal. Calcd. for $C_{24}H_{22}N_8O_2S$ (486.55): C, 59.25; H, 4.56; N, 23.03. Found: C, 59.08; H, 4.47; N, 22.89%.

4.1.3.6. 4-(2-(Bis([1, 2, 4]triazolo)[4,3-a:3′,4′-c]quinoxalin-3-ylthio)acetamido)-N-cyclohexylbenzamide (23f). White crystal (yield, 70%); m.p. = 270–272 °C. FT-IR (ν_{max}, cm^{-1}): 3269, 3131 (NH), 2930 (CH aliphatic), 1700, 1633 (C=O), 1607 (C=N); ^{1}H NMR (700 MHz, DMSO-d_6) δ 10.68 (s, 1H), 10.02 (s, 1H), 8.61 (dd, J = 7.9, 1.6 Hz, 1H), 8.47 (dd, J = 7.7, 1.8 Hz, 1H), 8.09 (d, J = 7.9 Hz, 1H), 7.82 (d, J = 8.6 Hz, 2H), 7.76 (dtd, J = 16.4, 7.5, 1.5 Hz, 2H), 7.65 (d, J = 8.7 Hz, 2H), 4.57 (s, 2H), 3.75 (ddt, J = 15.1, 11.0, 5.3 Hz, 1H), 1.81 (dt, J = 8.6, 4.1 Hz, 2H), 1.74 (dt, J = 11.4, 4.1 Hz, 2H), 1.64 – 1.59 (m, 1H), 1.30 (dd, J = 11.3, 8.6 Hz, 4H), 1.13 (qt, J = 8.4, 4.3 Hz, 1H); ^{13}C NMR (176 MHz, DMSO-d_6) δ 165.88, 165.14, 147.73, 142.12, 141.54, 139.36, 138.78, 130.21, 128.69 (2C), 128.37, 128.35,

124.10, 123.22, 118.67 (2C), 118.59, 118.07, 48.73, 38.87, 32.95 (2C), 25.76, 25.45 (2C); MS (*m/z*): 501 (M^+ + 1, 100%); Anal. Calcd. for $C_{25}H_{24}N_8O_2S$ (500.58): C, 59.99; H, 4.83; N, 22.39. Found: C, 59.85; H, 4.76; N, 22.11%.

4.1.3.7. N-(4-Acetylphenyl)-4-(2-(bis([1, 2, 4]triazolo)[4,3-a:3′,4′-c]quinoxalin-3-ylthio)acetamido)benzamide (23g). Pale white crystal (yield, 80%); m.p. = 275–277 °C. FT-IR (ν_{max}, cm^{-1}): 3300 (NH), 1655 (C=O), 1593 (C=N); ^{1}H NMR (700 MHz, DMSO-d_6) δ 10.77 (s, 1H), 10.14 (s, 1H), 7.97 (d, J = 8.6 Hz, 2H), 7.81 (dd, J = 8.0, 1.5 Hz, 1H), 7.78 – 7.76 (m, 2H), 7.72 (d, J = 8.7 Hz, 2H), 7.59 – 7.57 (m, 1H), 7.54 (dd, J = 8.5, 1.3 Hz, 1H), 7.40 – 7.37 (m, 1H), 7.36 – 7.34 (m, 2H), 7.10 (t, J = 7.4 Hz, 1H), 5.19 (s, 2H), 2.49 (s, 3H); ^{13}C NMR (176 MHz, DMSO-d_6) δ 165.80, 165.23, 157.97, 154.85, 142.00, 139.71, 133.48, 132.47 (2C), 130.20 (2C), 130.04, 129.29, 129.23 (2C), 129.05 (2C), 123.99, 123.94 (2C), 120.80 (2C), 118.83 (2C), 115.21, 45.80, 21.59; MS (*m/z*): 537 (M^+ + 1, 40%), 354 (40%); Anal. Calcd. for $C_{27}H_{20}N_8O_3S$ (536.57): C, 60.44; H, 3.76; N, 20.88. Found: C, 60.10; H, 3.66; N, 20.59%.

4.1.3.8. 4-(2-(Bis([1, 2, 4]triazolo)[4,3-a:3′,4′-c]quinoxalin-3-ylthio)acetamido)-N-(3-chlorophenyl)benzamide (23h). Yellowish white crystal (yield, 63%); m.p. = 280–282 °C. FT-IR (ν_{max}, cm^{-1}): 3267, 3109 (NH), 1701, 1647 (C=O), 1593 (C=N); ^{1}H NMR (700 MHz, DMSO-d_6) δ 10.79 (s, 1H), 10.30 (s, 1H), 10.02 (s, 1H), 8.61 (dd, J = 8.1, 1.5 Hz, 1H), 8.47 (dd, J = 7.9, 1.7 Hz, 1H), 7.98 – 7.95 (m, 3H), 7.78 – 7.73 (m, 4H), 7.70 (ddd, J = 8.3, 2.1, 1.0 Hz, 1H), 7.38 (t, J = 8.1 Hz, 1H), 7.15 (ddd, J = 8.0, 2.1, 0.9 Hz, 1H), 4.59 (s, 2H); ^{13}C NMR (176 MHz, DMSO-d_6) δ 166.08, 165.52, 147.71, 142.38, 142.12, 141.23, 139.34, 138.78, 133.38, 130.76, 129.63, 129.30 (2C), 128.37, 124.08, 123.65, 123.20, 120.10 (2C), 119.03, 118.86 (2C), 118.59, 118.06, 38.89; Anal. Calcd. for $C_{25}H_{17}ClN_8O_2S$ (528.98): C, 56.77; H, 3.24; N, 21.18. Found: C, 56.37; H, 3.11; N, 20.99%.

4.1.3.9. 4-(2-(Bis([1, 2, 4]triazolo)[4,3-a:3′,4′-c]quinoxalin-3-ylthio)acetamido)-N-(4-chlorophenyl)benzamide (23i). Yellow crystal (yield, 65%); m.p. = 277–279 °C. FT-IR (ν_{max}, cm^{-1}): 3382, 3111 (NH), 1674 (C=O), 1595 (C=N); ^{1}H NMR (700 MHz, DMSO-d_6) δ 10.78 (s, 1H), 10.28 (s, 1H), 10.03 (s, 1H), 8.62 (d, J = 8.0 Hz, 1H), 8.53 – 8.44 (m, 1H), 7.96 (d, J = 8.5 Hz, 3H), 7.82 (d, J = 8.5 Hz, 2H), 7.78 (d, J = 9.1 Hz, 1H), 7.74 (d, J = 8.4 Hz, 2H), 7.41 (d, J = 8.6 Hz, 2H), 4.59 (s, 2H); ^{13}C NMR (176 MHz, DMSO-d_6) δ 166.07, 165.39, 147.71, 142.29, 142.15, 139.37, 138.79, 138.72, 129.80, 129.26 (2C), 128.98 (2C), 128.38 (2C), 127.57, 124.12, 123.24, 122.27 (2C), 118.86 (2C), 118.61, 118.08, 38.88; Anal. Calcd. for $C_{25}H_{17}ClN_8O_2S$ (528.98): C, 56.77; H, 3.24; N, 21.18. Found: C, 56.44; H, 3.19; N, 20.85%.

4.1.3.10. 4-(2-(Bis([1, 2, 4]triazolo)[4,3-a:3′,4′-c]uinoxaline-3-ylthio)acetamido)-N-(2,5-dichlorophenyl)benzamide (23j). White crystal (yield, 78%); m.p. = 260–262 °C. FT-IR (ν_{max}, cm^{-1}): 3429 (NH), 1672 (C=O), 1511 (C=N); ^{1}H NMR (700 MHz, DMSO-d_6) δ 10.80 (s, 1H), 10.03 (s, 2H), 8.62 (dd, J = 8.0, 1.5 Hz, 1H), 8.48 (dd, J = 7.9, 1.7 Hz, 1H), 7.99 – 7.97 (m, 2H), 7.77 (dt, J = 5.0, 2.2 Hz, 2H), 7.76 (m, 2H), 7.75 (s, 1H), 7.61 (d, J = 8.6 Hz, 1H), 7.38 (dd, J = 8.6, 2.6 Hz, 1H), 4.60 (s, 2H); ^{13}C NMR (176 MHz, DMSO-d_6) δ 166.11, 165.23, 147.70, 142.59, 142.15, 139.37, 138.79, 136.95, 131.89, 131.35, 129.39 (2C), 128.76, 128.39, 128.37, 128.20, 127.90, 127.39, 124.11, 123.23, 118.94 (2C), 118.60, 118.08, 38.89; MS (*m/z*): 563 (M^+, 30%), 420 (65%); Anal. Calcd. For $C_{25}H_{16}Cl_2N_8O_2S$ (563.42): C, 53.30; H, 2.86; N, 19.89. Found: C, 53.01; H, 2.77; N, 19.66%.

4.1.3.11. 4-(2-(Bis([1, 2, 4]triazolo)[4,3-a:3′,4′-c]uinoxaline-3-ylthio)acetamido)-N-(4-fluorophenyl)benzamide (23k). White powder (yield, 80%); m.p. = 250–252 °C. FT-IR (ν_{max}, cm^{-1}): 3289, 3108 (NH), 1645 (C=O), 1604 (C=N); ^{1}H NMR (700 MHz, DMSO-d_6) δ 10.77 (s, 1H), 10.21 (s, 1H), 10.02 (s, 1H), 8.79 – 8.57 (m, 1H), 8.55 – 8.41 (m, 1H), 7.96 (t, J = 9.5 Hz, 2H), 7.78 (dt, J = 35.0, 12.1 Hz, 5H), 7.26 – 7.14 (m, 3H), 4.59 (s, 2H); ^{13}C NMR (176 MHz, DMSO-d_6) δ 166.04, 165.20, 147.72, 142.11, 139.34, 138.78, 129.17 (2C), 128.36 (2C), 124.08, 123.19, 122.61 (2C), 122.57 (2C), 118.84 (2C), 118.58, 118.06, 115.68 (2C), 115.55 (2C), 38.90; MS (*m/z*): 513 (M^+ + 1, 25%), 372 (100%); Anal. Calcd. For $C_{25}H_{17}FN_8O_2S$ (512.52): C, 58.59; H, 3.34; N, 21.86. Found: C, 58.34; H, 3.22; N, 21.69%.

4.1.3.12. 4-(2-(Bis([1, 2, 4]triazolo)[4,3-a:3′,4′-c]uinoxaline-3-ylthio)acetamido)-N-(2-hydroxyphenyl)benzamide (23l). Off white crystal (yield, 71%); m.p. = 282–284 °C. FT-IR (ν_{max}, cm^{-1}): 3263 (NH), 1646 (C=O), 1600 (C=N); ^{1}H NMR (700 MHz, DMSO-d_6) δ 10.78 (s, 1H), 10.02 (s, 1H), 9.76 (s, 1H), 9.46 (s, 1H), 8.60 (dd, J = 8.1, 1.4 Hz, 1H), 8.46 (dd, J = 8.0, 1.7 Hz, 1H), 7.97 – 7.96 (m, 2H), 7.75 – 7.73 (m, 3H), 7.69 (dt, J = 8.1, 2.1 Hz, 2H), 7.04 – 7.03 (m, 1H), 6.93 – 6.92 (m, 1H), 6.84 – 6.83 (m, 1H), 4.60 (s, 2H); ^{13}C NMR (176 MHz, DMSO-d_6) δ 166.05, 165.10, 149.68, 147.72, 142.24, 142.10, 139.33, 138.77, 129.49, 129.08 (2C), 128.36, 128.34, 126.46, 126.03, 124.43, 124.06, 123.17, 119.53 (2C), 118.95, 118.57, 118.06, 116.50, 38.93; MS (*m/z*): 511 (M^+ + 1, 70%), 293 (100%); Anal. Calcd. For $C_{25}H_{18}N_8O_3S$ (510.53): C, 58.82; H, 3.55; N, 21.95. Found: C, 58.78; H, 3.50; N, 21.88%.

4.1.3.13. 4-(2-(Bis([1, 2, 4]triazolo)[4,3-a:3′,4′-c]uinoxaline-3-ylthio)acetamido)-N-(4-hydroxyphenyl)benzamide (23m). Pale yellow crystal (yield, 75%); m.p. = 285–287 °C. FT-IR (ν_{max}, cm^{-1}): 3414 (NH), 1601 (C=N); ^{1}H NMR (700 MHz, DMSO-d_6) δ 10.75 (s, 1H), 10.01 (s, 1H), 9.93 (s, 1H), 9.26 (s, 1H), 8.63 – 8.54 (m, 1H), 8.51 – 8.39 (m, 1H), 7.93 (d, J = 8.7 Hz, 2H), 7.72 (dq, J = 14.7, 7.1, 6.6 Hz, 4H), 7.55 – 7.49 (m, 2H), 6.79 – 6.70 (m, 2H), 4.59 (s, 2H); ^{13}C NMR (176 MHz, DMSO-d_6) δ 165.99, 164.72, 154.09 (2C), 147.74, 142.05, 139.30, 138.77, 131.21, 130.33, 128.98 (2C), 128.33 (2C), 124.01, 123.12, 122.74 (2C), 118.81(2C), 118.55, 118.02, 115.42 (2C), 38.92; MS (*m/z*): 511(M^+ + 1, 30%); Anal. Calcd. For $C_{25}H_{18}N_8O_3S$ (510.53): C, 58.82; H, 3.55; N, 21.95. Found: C, 58.63; H, 3.48; N, 21.73%.

4.1.3.14. 4-(2-(Bis([1, 2, 4]triazolo)[4,3-a:3′,4′-c]uinoxaline-3-ylthio)acetamido)-N-(2-hydroxy-4-nitrophenyl)benzamide (23n). Red crystal (yield, 68%); m.p. = 265–267 °C. FT-IR (ν_{max}, cm^{-1}): 3294, 3101 (NH), 2927 (CH aliphatic), 1653 (C=O), 1603 (C=N); ^{1}H NMR (700 MHz, DMSO-d_6) δ 11.14 (s, 1H), 10.82 (s, 1H), 10.02 (s, 1H), 9.49 (s, 1H), 8.61 (dd, J = 8.1, 1.5 Hz, 1H), 8.47 (dd, J = 7.8, 1.8 Hz, 1H), 8.25 (d, J = 8.9 Hz, 1H), 7.98 – 7.96 (m, 2H), 7.79 (dd, J = 8.9, 2.6 Hz, 1H), 7.78 – 7.75 (m, 3H), 7.74 (dd, J = 6.7, 2.1 Hz, 2H), 4.60 (s, 2H); ^{13}C NMR (176 MHz, DMSO-d_6) δ 166.14, 165.06, 148.55, 147.70, 143.66, 142.72, 142.13, 139.35, 138.78, 133.63, 129.27 (2C), 128.90, 128.38, 128.36, 124.08, 123.20, 121.83, 119.05 (2C), 118.59, 118.07, 115.57, 109.89, 38.91; MS (*m/z*): 554 (M^+ – 1, 70%); Anal. Calcd. For $C_{25}H_{17}N_9O_5S$ (555.53): C, 54.05; H, 3.08; N, 22.69. Found: C, 53.85; H, 2.97; N, 22.43%.

4.1.4. General procedure for the synthesis of compounds 24a–c

A mixture of potassium salt of bis([1, 2, 4]triazolo)[4,3-*a*:3′,4′-*c*]quinoxaline-3-thiol **14** (0.5 g, 0.001 mol) and 2-chloro-*N*-(4–(2-

(substituted)hydrazine-1-carbonyl)phenyl)acetamide **22a–c** (0.001 mol) in DMF (50 ml) was heated on a water bath for 6 h. After cooling to room temperature, the reaction mixture was poured on crushed ice. The obtained precipitates were collected by filtration, dried, and crystalised from ethanol to give the target compounds **24a–c.**

4.1.4.1. 2-(Bis([1, 2, 4]triazolo)[4,3-a:3′,4′-c]quinoxalin-3-ylthio)-N-(4–(2-(2-chlorobenzoyl)hydrazine-1-carbonyl)phenyl)acetamide (24a).

White crystal (yield, 65%); m.p. = 220–222 °C. FT-IR (ν_{max}, cm^{-1}): 3185 (NH), 1698 (C=O), 1603 (C=N); ^{1}H NMR (700 MHz, DMSO-d_6) δ 10.77 (s, 1H), 10.54 (s, 1H), 10.37 (s, 1H), 10.03 (s, 1H), 8.63 (dd, J = 8.1, 1.5 Hz, 1H), 8.48 (dd, J = 7.9, 1.7 Hz, 1H), 7.93 (d, J = 8.7 Hz, 2H), 7.77 (dtd, J = 17.1, 7.5, 1.5 Hz, 2H), 7.72 (d, J = 8.7 Hz, 2H), 7.57 (ddd, J = 8.0, 4.0, 1.5 Hz, 2H), 7.53 (td, J = 7.6, 1.7 Hz, 1H), 7.48 (td, J = 7.4, 1.3 Hz, 1H), 4.60 (s, 2H); ^{13}C NMR (176 MHz, DMSO-d_6) δ 166.25, 166.08, 165.40, 147.70, 142.36, 142.15, 139.37, 138.79, 135.18, 131.98, 130.93, 130.38, 129.90, 129.06 (2C), 128.37 (2C), 127.64 (2C), 124.12, 123.23, 118.91(2C), 118.60, 118.10, 38.94. MS (*m/z*): 572 (M^+, 100%); Anal. Calcd. for $C_{26}H_{18}ClN_9O_3S$ (572): C, 54.60; H, 3.17; N, 22.04. Found: C, 54.39; H, 3.09; N, 21.88%.

4.1.4.2. 2-(Bis([1, 2, 4]triazolo)[4,3-a:3′,4′-c]quinoxalin-3-ylthio)-N-(4–(2-(3-chlorobenzoyl)hydrazine-1-carbonyl)phenyl)acetamide (24b).

White crystal (yield, 63%); m.p. = 232–234 °C. FT-IR (ν_{max}, cm^{-1}): 3260, 3108 (NH), 1639 (C=O), 1603 (C=N); ^{1}H NMR (700 MHz, DMSO-d_6) δ 10.78 (s, 1H), 10.62 (s, 1H), 10.49 (s, 1H), 10.02 (s, 1H), 8.62 (dd, J = 8.0, 1.5 Hz, 1H), 8.47 (dd, J = 7.8, 1.7 Hz, 1H), 7.96 (t, J = 1.9 Hz, 1H), 7.92 (d, J = 8.5 Hz, 2H), 7.91 – 7.88 (m, 1H), 7.78 – 7.76 (m, 1H), 7.75 – 7.71 (m, 3H), 7.70 – 7.69 (m, 1H), 7.59 (t, J = 7.9 Hz, 1H), 4.60 (s, 2H); ^{13}C NMR (176 MHz, DMSO-d_6) δ 166.09, 165.67, 164.99, 147.71, 142.40, 142.13, 139.35, 138.78, 135.00, 133.84, 132.23, 131.11, 129.03 (2C), 128.38, 128.36, 127.72 (2C), 127.66, 126.66, 124.09, 123.21, 118.96, 118.59, 118.07, 38.92; MS (*m/z*): 572 (M^+, 100%); Anal. Calcd. for $C_{26}H_{18}ClN_9O_3S$ (572): C, 54.60; H, 3.17; N, 22.04. Found: C, 54.45; H, 3.11; N, 21.95%.

4.1.4.3. 2-(Bis([1, 2, 4]triazolo)[4,3-a:3′,4′-c]quinoxalin-3-ylthio)-N-(4–(2-(2-hydroxybenzoyl)hydrazine-1-carbonyl)phenyl)acetamide (24c).

Yellow crystal (yield, 60%); m.p. = 270–272 °C. FT-IR (ν_{max}, cm^{-1}): 3282 (NH), 1648, 1619 (C=O), 1599 (C=N); ^{1}H NMR (700 MHz, DMSO-d_6) δ 11.96 (s, 1H), 10.78 (s, 1H), 10.67 (s, 1H), 10.59 (s, 1H), 10.02 (s, 1H), 8.62 (dd, J = 8.0, 1.5 Hz, 1H), 8.47 (dd, J = 7.8, 1.7 Hz, 1H), 7.93 (dd, J = 10.4, 7.6 Hz, 3H), 7.77 (ddt, J = 10.8, 8.3, 3.9 Hz, 2H), 7.74 (dd, J = 7.3, 4.8 Hz, 2H), 7.47 (ddd, J = 8.7, 7.2, 1.7 Hz, 1H), 7.00 – 6.95 (m, 2H), 4.59 (s, 2H); ^{13}C NMR (176 MHz, DMSO-d_6) δ 168.26, 166.09, 165.44, 159.79, 147.71, 142.45, 142.13, 139.35, 138.78, 134.65, 129.07 (2 C), 128.73, 128.38, 128.36, 127.52, 124.09, 123.21, 119.52, 118.96 (2C), 118.59, 118.07, 117.88, 115.01, 38.91; MS (*m/z*): 554 (M^+ + 1, 100%); Anal. Calcd. for $C_{26}H_{19}N_9O_4S$ (553.56): C, 56.41; H, 3.46; N, 22.77. Found: C, 56.20; H, 3.39; N, 22.58%.

4.2. Biological testing

4.2.1. In vitro anti-proliferative activity

MTT assay protocol[55–57,74] was applied as described in Supplementary data.

4.2.2. In vitro VEGFR-2 kinase assay

All the synthesised compounds were tested for their inhibitory activity against VEGFR-2 as described in Supplementary data[75].

4.2.3. Flow cytometry analysis for cell cycle

Cell cycle analysis was performed using propidium iodide (PI) staining and flow cytometry analysis for compound **23j** as described in Supplementary data[76,77].

4.2.4. Flow cytometry analysis for apoptosis

Apoptotic effect was assessed for compound **23j** as described in Supplementary data[78,79].

4.2.5. Western blot analysis

Western blot technique was performed for compound **23j** to determine its effect against caspase3, caspase9, BAX, and Bcl-2 as described in Supplementary data[80–82].

4.3. In silico studies

4.3.1. Docking studies

Docking studies were carried out against VEEGFR-2 (PDB ID: 2OH4) using Discovery Studio 4.0 as described in Supplementary data[83–85,86,87].

4.3.2. Admet studies

ADMET studies were carried out as described in Supplementary data[85,87].

4.3.3. Toxicity studies

Toxicity studies were performed as described in Supplementary data.

Acknowledgements

The authors extend their appreciation to the Deanship ofScientific Research at King Saud University for funding this workthrough research group no [RG-1441–364].

Disclosure statement

No potential conflict of interest was reported by the author(s). The authors would like to acknowledge Dr. Mohamed R. Elnagar, Department of Pharmacology and Toxicology, Faculty of Pharmacy, Al-Azhar University, Cairo, Egypt for his valuable suggestion and technical assistance.

Funding

The authors extend their appreciation to the Deanship of Scientific Research at King Saud University for funding this work through research group no [RG-1441–364].

ORCID

Nawaf A. Alsaif http://orcid.org/0000-0001-9215-1380
Mohammed S. Taghour http://orcid.org/0000-0003-0630-709X

Mohammed M. Alanazi http://orcid.org/0000-0002-0483-8113
Ahmad J. Obaidullah http://orcid.org/0000-0002-7532-6318
Abdulrahman A. Al-Mehizia http://orcid.org/0000-0001-8711-3873
Alaa Elwan http://orcid.org/0000-0003-4270-616X
Hazem Elkady http://orcid.org/0000-0003-0893-6703

References

1. Madani I, De Neve W, Mareel M. Does ionizing radiation stimulate cancer invasion and metastasis? Bulletin du Cancer 2008;95:292–300.
2. Konsoulova A. Principles of cancer immunobiology and immunotherapy of solid tumors, Immunopathology and immunomodulation. Rijeka (Croatia): InTech; 2015:77–99.
3. Jadala C, Sathish M, Reddy TS, et al. Synthesis and in vitro cytotoxicity evaluation of β-carboline-combretastatin carboxamides as apoptosis inducing agents: DNA intercalation and topoisomerase-II inhibition. Bioorg Med Chem 2019;27:3285–98.
4. Jafari F, Baghayi H, Lavaee P, et al. Design, synthesis and biological evaluation of novel benzo-and tetrahydrobenzo-[h] quinoline derivatives as potential DNA-intercalating antitumor agents. Eur J Med Chem 2019;164:292–303.
5. El-Adl K, El-Helby A-GA, Sakr H, et al. Design, synthesis, molecular docking and anticancer evaluations of 5-benzylidenethiazolidine-2,4-dione derivatives targeting VEGFR-2 enzyme . Bioorg Chem 2020;102:104059.
6. Shen F-Q, Shi L, Wang Z-F, et al. Design, synthesis, biological evaluation of benzoyl amide derivatives containing nitrogen heterocyclic ring as potential VEGFR-2 inhibitors. Bioorg Med Chem 2019;27:3813–24.
7. Fan H, Wei D, Zheng K, et al. Discovery of dioxino[2,3-f]quinazoline derivative VEGFR-2 inhibitors exerting significant antipro-liferative activity in HUVECs and mice . Eur J Med Chem 2019;175:349–56.
8. Yuan X, Yang Q, Liu T, et al. Design, synthesis and in vitro evaluation of 6-amide-2-aryl benzoxazole/benzimidazole derivatives against tumor cells by inhibiting VEGFR-2 kinase . Eur J Med Chem 2019;179:147–65.
9. Ribatti D, Vacca A, Dammacco F. The role of the vascular phase in solid tumor growth: a historical review. Neoplasia 1999;1:293–302.
10. Nagy J, Chang S, Dvorak A, Dvorak H. Why are tumour blood vessels abnormal and why is it important to know? Br J Cancer 2009;100:865–9.
11. Zirlik K, Duyster J. Anti-angiogenics: current situation and future perspectives. Oncol Res Treat 2018;41:166–71.
12. Sullivan LA, Brekken RA. The VEGF family in cancer and antibody-based strategies for their inhibition, MAbs. London, UK: Taylor & Francis; 2010: 165–175.
13. Bagnasco L, Piras D, Parodi S, et al. Role of angiogenesis inhibitors in colorectal cancer: sensitive and insensitive tumors. Curr Cancer Drug Targets 2012;12:303–15.
14. Gotink KJ, Verheul HM. Anti-angiogenic tyrosine kinase inhibitors: what is their mechanism of action? Angiogenesis 2010;13:1–14.
15. Modi SJ, Kulkarni VM. Vascular endothelial growth factor receptor (VEGFR-2)/KDR inhibitors: medicinal chemistry perspective. Med Drug Discov 2019;2:100009.
16. Yadav L, Puri N, Rastogi V, et al. Tumour angiogenesis and angiogenic inhibitors: a review. J Clin Diagn Res 2015;9:XE01–XE05.
17. Sobhy MK, Mowafy S, Lasheen DS, et al. 3D-QSAR pharmacophore modelling, virtual screening and docking studies for lead discovery of a novel scaffold for VEGFR 2 inhibitors: design, synthesis and biological evaluation. Bioorg Chem 2019;89:102988.
18. Niu G, Chen X. Vascular endothelial growth factor as an anti-angiogenic target for cancer therapy. Curr Drug Targets 2010;11:1000–17.
19. Shibuya M. Vascular endothelial growth factor (VEGF) and its receptor (VEGFR) signaling in angiogenesis: a crucial target for anti- and pro-angiogenic therapies. Genes & Cancer 2011;2:1097–105.
20. Roskoski R Jr. Vascular endothelial growth factor (VEGF) signaling in tumor progression. Crit Rev Oncol/Hematol 2007;62:179–213.
21. Marzouk AA, Abdel-Aziz SA, Abdelrahman KS, et al. Design and synthesis of new 1,6-dihydropyrimidin-2-thio derivatives targeting VEGFR-2: molecular docking and antiproliferative evaluation . Bioorg Chem 2020;102:104090.
22. Ge Y-L, Zhang X, Zhang J-Y, et al. The mechanisms on apoptosis by inhibiting VEGF expression in human breast cancer cells. Int Immunopharmacol 2009;9:389–95.
23. Ghorab MM, Alsaid MS, Soliman AM, Ragab FA. VEGFR-2 inhibitors and apoptosis inducers: synthesis and molecular design of new benzo[g]quinazolin bearing benzenesulfonamide moiety. J Enzyme Inhib Med Chem 2017;32:893–907.
24. El-Gazzar MG, El-Hazek RM, Zaher NH, El-Ghazaly MA. Design and synthesis of novel pyridazinoquinazoline derivatives as potent VEGFR-2 inhibitors: in vitro and in vivo study. Bioorg Chem 2019;92:103251.
25. Fukumura D, Kloepper J, Amoozgar Z, et al. Enhancing cancer immunotherapy using antiangiogenics: opportunities and challenges. Nat Rev Clin Oncol 2018;15:325–40.
26. Zaman S, Wang R, Gandhi V. Targeting the apoptosis pathway in hematologic malignancies. Leuk Lymphoma 2014;55:1980–92.
27. Ragab FA, Nissan YM, Seif EM, et al. Synthesis and in vitro investigation of novel cytotoxic pyrimidine and pyrazolopyrimidne derivatives showing apoptotic effect. Bioorg Chem 2020;96:103621.
28. AbdelHaleem A, Mansour AO, AbdelKader M, Arafa RK. Selective VEGFR-2 inhibitors: synthesis of pyridine derivatives, cytotoxicity and apoptosis induction profiling. Bioorg Chem 2020;103:104222.
29. Lee K, Jeong K-W, Lee Y, et al. Pharmacophore modeling and virtual screening studies for new VEGFR-2 kinase inhibitors. Eur J Med Chem 2010;45:5420–7.
30. Xie Q-Q, Xie H-Z, Ren J-X, et al. Pharmacophore modeling studies of type I and type II kinase inhibitors of Tie2. J Mol Graph Model 2009;27:751–8.
31. Eskander RN, Tewari KS. Incorporation of anti-angiogenesis therapy in the management of advanced ovarian carcinoma-mechanistics, review of phase III randomized clinical trials, and regulatory implications. Gynec Oncol 2014;132:496–505.
32. Machado VA, Peixoto D, Costa R, et al. Synthesis, antiangiogenesis evaluation and molecular docking studies of 1-aryl-3-[(thieno [3, 2-b] pyridin-7-ylthio) phenyl] ureas: discovery of a new substitution pattern for type II VEGFR-2 Tyr kinase inhibitors. Bioorg Med Chem 2015;23:6497–509.
33. Wang Z, Wang N, Han S, et al. Dietary compound isoliquiritigenin inhibits breast cancer neoangiogenesis via VEGF/VEGFR-2 signaling pathway. PLOS One 2013;8:e68566.

34. Dietrich J, Hulme C, Hurley LH. The design, synthesis, and evaluation of 8 hybrid DFG-out allosteric kinase inhibitors: a structural analysis of the binding interactions of Gleevec®, Nexavar®, and BIRB-796. Bioorg Med Chem 2010;18:5738–48.
35. Wilhelm S, Carter C, Lynch M, et al. Discovery and development of sorafenib: a multikinase inhibitor for treating cancer. Nat Rev Drug Discov 2006;5:835–44.
36. Lintnerová L, García-Caballero M, Gregáň F, et al. A development of chimeric VEGFR2 TK inhibitor based on two ligand conformers from PDB: 1Y6A complex-medicinal chemistry consequences of a TKs analysis. Eur J Med Chem 2014;72: 146–59.
37. Matsui J, Funahashi Y, Uenaka T, et al. Multi-kinase inhibitor E7080 suppresses lymph node and lung metastases of human mammary breast tumor MDA-MB-231 via inhibition of vascular endothelial growth factor-receptor (VEGF-R) 2 and VEGF-R3 kinase. Clin Cancer Res 2008;14:5459–65.
38. Peng F-W, Liu D-K, Zhang Q-W, et al. VEGFR-2 inhibitors and the therapeutic applications thereof: a patent review (2012-2016). Expert Opin Ther Pat 2017;27:987–1004.
39. Zhang Y, Zou J-Y, Wang Z, Wang Y. Fruquintinib: a novel antivascular endothelial growth factor receptor tyrosine kinase inhibitor for the treatment of metastatic colorectal cancer. Cancer Manage Res 2019;11:7787–803.
40. Mahdy HA, Ibrahim MK, Metwaly AM, et al. Design, synthesis, molecular modeling, in vivo studies and anticancer evaluation of quinazolin-4(3H)-one derivatives as potential VEGFR-2 inhibitors and apoptosis inducers . Bioorg Chem 2020;94:103422.
41. Eissa IH, El-Helby A-GA, Mahdy HA, et al. Discovery of new quinazolin-4(3H)-ones as VEGFR-2 inhibitors: design, synthesis, and anti-proliferative evaluation . Bioorg Chem 2020;105: 104380.
42. El-Zahabi MA, Sakr H, El-Adl K, et al. Design, synthesis, and biological evaluation of new challenging thalidomide analogs as potential anticancer immunomodulatory agents. Bioorg Chem 2020;104:104218.
43. Elmetwally SA, Saied KF, Eissa IH, Elkaeed EB. Design, synthesis and anticancer evaluation of thieno[2,3-d]pyrimidine derivatives as dual EGFR/HER2 inhibitors and apoptosis inducers . Bioorg Chem2019;88:102944.
44. Ibrahim M, Taghour M, Metwaly A, et al. Design, synthesis, molecular modeling and anti-proliferative evaluation of novel quinoxaline derivatives as potential DNA intercalators and topoisomerase II inhibitors. Eur J Med Chem 2018;155: 117–34.
45. Eldehna WM, Abo-Ashour MF, Nocentini A, et al. Novel 4/3-((4-oxo-5-(2-oxoindolin-3-ylidene)thiazolidin-2-ylidene)amino) benzenesulfonamides: Synthesis, carbonic anhydrase inhibitory activity, anticancer activity and molecular modelling studies . Eur J Med Chem 2017;139:250–62.
46. Eissa IH, El-Naggar AM, El-Hashash MA. Design, synthesis, molecular modeling and biological evaluation of novel 1H-pyrazolo [3, 4-b] pyridine derivatives as potential anticancer agents. Bioorg Chem 2016;67:43–56.
47. El-Naggar AM, Abou-El-Regal MM, El-Metwally SA, et al. Synthesis, characterization and molecular docking studies of thiouracil derivatives as potent thymidylate synthase inhibitors and potential anticancer agents. Mol Divers 2017;21: 967–83.
48. Alsaif NA, Dahab MA, Alanazi MM, et al. New quinoxaline derivatives as VEGFR-2 inhibitors with anticancer and apoptotic activity: design, molecular modeling, and synthesis. Bioorg Chem 2021;110:104807.
49. Romer DR. Synthesis of 2, 3-dichloroquinoxalines via Vilsmeier reagent chlorination. J Heterocycl Chem 2009;46: 317–9.
50. Sarges R, Howard HR, Browne RG, et al. 4-Amino[1,2,4]triazolo[4,3-a]quinoxalines. A novel class of potent adenosine receptor antagonists and potential rapid-onset antidepressants . J Med Chem 1990;33:2240–54.
51. Könnecke A, Lippmann E. Kondensierte Chinoxaline aus 2-Chlor-3-hydrazinochinoxalin. Zeitschrift Für Chemie 2010;18: 92–3.
52. Kanhed AA, Mehere AP, Pandey KR, Mahapatra DK. 4-(2-chloroacetamido) Benzoic acid derivatives as local anesthetic agents: design, synthesis, and characterization. UK J Pharm Biosci 2016;4:35–44.
53. El-Helby A-GA, Ayyad RR, El-Adl K, Elkady H. Phthalazine-1,4-dione derivatives as non-competitive AMPA receptor antagonists: design, synthesis, anticonvulsant evaluation, ADMET profile and molecular docking . Mol Divers 2019;23:283–98.
54. El-Helby AGA, Ayyad RR, Zayed MF, et al. Design, synthesis, in silico ADMET profile and GABA-A docking of novel phthalazines as potent anticonvulsants. Archiv Der Pharmazie 2019;352:1800387.
55. Mosmann T. Rapid colorimetric assay for cellular growth and survival: application to proliferation and cytotoxicity assays. J Immunol Methods 1983;65:55–63.
56. Denizot F, Lang R. Rapid colorimetric assay for cell growth and survival. Modifications to the tetrazolium dye procedure giving improved sensitivity and reliability. J Immunol Methods 1986;89:271–7.
57. Thabrew M, HUGHES RD, MCFARLANE IG. Screening of hepatoprotective plant components using a HepG2 cell cytotoxicity assay. J Pharm Pharmacol 2011;49:1132–5.
58. Liu Y, Gray NS. Rational design of inhibitors that bind to inactive kinase conformations. Nat Chem Biol 2006;2:358–64.
59. Klopman G, Stefan LR, Saiakhov RD. ADME evaluation. 2. A computer model for the prediction of intestinal absorption in humans. Eur J Pharm Sci 2002;17:253–63.
60. Mannhold R, Kubinyi H, Folkers G Pharmacokinetics and metabolism in drug design. Weinheim, Germany: John Wiley & Sons; 2012.
61. Roy PP, Roy K. QSAR studies of CYP2D6 inhibitor aryloxypropanolamines using 2D and 3D descriptors. Chem Biol Drug Des 2009;73:442–55.
62. Ghafourian T, Amin Z. QSAR models for the prediction of plasma protein binding. BioImpacts: BI 2013;3:21.
63. Van De Waterbeemd H, Gifford E. ADMET in silico modelling: towards prediction paradise? Nat Rev Drug Discov 2003;2: 192–204.
64. Xia X, Maliski EG, Gallant P, Rogers D. Classification of kinase inhibitors using a Bayesian model. J Med Chem 2004;47: 4463–70.
65. BIOVIA. QSAR, ADMET and Predictive Toxicology. https://www.3dsbiovia.com/products/collaborative-science/biovia-discovery-studio/qsar-admet-and-predictive-toxicology.html [last accessed May 2020]
66. Peto R, Pike M C, Bernstein L, et al. The TD50: a proposed general convention for the numerical description of the carcinogenic potency of chemicals in chronic-exposure animal experiments. Environ Health Perspect 1984; 58, 1–8.

67. Goodman G, Wilson R. Comparison of the dependence of the TD50 on maximum tolerated dose for mutagens and nonmutagens. Risk Anal 1992;12:525–33.
68. Council NR. Correlation between carcinogenic potency and the maximum tolerated dose: implications for risk assessment, issues in risk assessment. USA: National Academies Press; 1993.
69. Louisse J, Bosgra S, Blaauboer BJ, et al. Prediction of in vivo developmental toxicity of all-trans-retinoic acid based on in vitro toxicity data and in silico physiologically based kinetic modeling. Arch Toxicol 2015;89:1135–48.
70. EPA. Guidelines for Developmental Toxicity Risk Assessment. https://www.epa.gov/sites/production/files/2014-11/documents/dev_tox.pdf [last accessed May 2020].
71. Diaza RG, Manganelli S, Esposito A, et al. Comparison of in silico tools for evaluating rat oral acute toxicity. SAR QSAR Environ Res 2015;26:1–27.
72. Pizzo F, Benfenati E. In silico models for repeated-dose toxicity (RDT): prediction of the no observed adverse effect level (NOAEL) and lowest observed adverse effect level (LOAEL) for drugs, in silico methods for predicting drug toxicity. New York: Springer; 2016:163–176.
73. Venkatapathy R, Moudgal CJ, Bruce RM. Assessment of the oral rat chronic lowest observed adverse effect level model in TOPKAT, a QSAR software package for toxicity prediction. J Chem Inform Comput Sci 2004;44:1623–9.
74. Al-Rashood ST, Hamed AR, Hassan GS, et al. Antitumor properties of certain spirooxindoles towards hepatocellular carcinoma endowed with antioxidant activity. J Enzyme Inhib Med Chem 2020;35:831–9.
75. Abou-Seri SM, Eldehna WM, Ali MM, Abou El Ella DA. 1-Piperazinylphthalazines as potential VEGFR-2 inhibitors and anticancer agents: synthesis and in vitro biological evaluation. Eur J Med Chem 2016;107:165–79.
76. Wang J, Lenardo MJ. Roles of caspases in apoptosis, development, and cytokine maturation revealed by homozygous gene deficiencies. J Cell Sci 2000;113:753–7.
77. Eldehna WM, Hassan GS, Al-Rashood ST, et al. Synthesis and in vitro anticancer activity of certain novel 1-(2-methyl-6-arylpyridin-3-yl)-3-phenylureas as apoptosis-inducing agents. J Enzyme Inhib Med Chem 2019;34:322–32.
78. Lo KK-W, Lee TK-M, Lau JS-Y, et al. Luminescent biological probes derived from ruthenium(II) estradiol polypyridine complexes. Inorg Chem 2008;47:200–8.
79. Sabt A, Abdelhafez OM, El-Haggar RS, et al. Novel coumarin-6-sulfonamides as apoptotic anti-proliferative agents: synthesis, in vitro biological evaluation, and QSAR studies. J Enzyme Inhib Med Chem 2018;33:1095–107.
80. Balah A, Ezzat O, Akool E-S. Vitamin E inhibits cyclosporin A-induced CTGF and TIMP-1 expression by repressing ROS-mediated activation of TGF-β/Smad signaling pathway in rat liver. Int Immunopharmacol 2018;65:493–502.
81. Aborehab NM, Elnagar MR, Waly NE. Gallic acid potentiates the apoptotic effect of paclitaxel and carboplatin via overexpression of Bax and P53 on the MCF-7 human breast cancer cell line. J Biochem Mol Toxicol 2021;35:e22638.
82. Elnagar MR, Walls AB, Helal GK, et al. Functional characterization of α7 nicotinic acetylcholine and NMDA receptor signaling in SH-SY5Y neuroblastoma cells in an ERK phosphorylation assay. Eur J Pharmacol 2018;826:106–13.
83. Ibrahim MK, Eissa IH, Abdallah AE, et al. Design, synthesis, molecular modeling and anti-hyperglycemic evaluation of novel quinoxaline derivatives as potential PPARγ and SUR agonists. Bioorg Med Chem 2017;25:1496–513.
84. El-Helby AGA, Ayyad RR, Sakr HM, et al. Design, synthesis, molecular modeling and biological evaluation of novel 2,3-dihydrophthalazine-1,4-dione derivatives as potential anticonvulsant agents. J Mol Struct 2017;1130:333–51.
85. Ibrahim MK, Eissa IH, Alesawy MS, et al. Design, synthesis, molecular modeling and anti-hyperglycemic evaluation of quinazolin-4(3H)-one derivatives as potential PPARγ and SUR agonists . Bioorg Med Chem 2017;25:4723–44.
86. El-Gamal KM, El-Morsy AM, Saad AM, et al. Synthesis, docking, QSAR, ADMET and antimicrobial evaluation of new quinoline-3-carbonitrile derivatives as potential DNA-gyrase inhibitors. J Mol Struct 2018;1166:15–33.
87. El-Zahabi MA, Elbendary ER, Bamanie FH, et al. Design, synthesis, molecular modeling and anti-hyperglycemic evaluation of phthalimide-sulfonylurea hybrids as PPARγ and SUR agonists. Bioorg Chem 2019;91:103115.